Modeling and Design of an Electric All-Terrain Vehicle

By:

Adam R. Chevrefils

A Thesis submitted to the Faculty of Graduate Studies of

The University of Manitoba

in partial fulfillment of the requirements for the degree of

MASTER OF SCIENCE

Department of Electrical and Computer Engineering

University of Manitoba

Winnipeg, Manitoba

ACKNOWLEDGEMENT

The author owes sincere gratitude to his academic advisor, Dr. Shaahin Filizadeh, for his continued support and encouragement throughout his graduate studies. Without Dr. Filizadeh's amiability and expertise, this endeavour would not have progressed as steadily as it has. A word of thanks is also owed to Mr. Erwin Dirks and the other support staff of the University of Manitoba.

Appreciation is due to the Manitoba HVDC Research Centre for their financial support. The technical expertise and experience of Mr. Randy Wachal, Mr. Farid Mosallat and Mr. Warren Erickson have been assets to the project.

Thanks are attributed to Polaris Industries for providing the all-terrain vehicle and hardware, which have made this project possible.

Funding from the Natural Sciences and Engineering Research Council (NSERC) is earnestly acknowledged

I would especially like to thank my family and friends, chiefly my loving and encouraging parents, for their support and understanding throughout the project. I would also like to extend a special thank you to my father and mother-in-law, Mr. & Mrs. Beaudry, for their support and encouragement throughout the project.

A special recognition is extended to Mr. Michel Bourgeois for his especial talents and countless hours contributed towards the mechanical conversion of the vehicle.

Lastly, to my wonderful wife Rachelle, who has provided incessant support and encouragement and whose sacrifices do not go unnoticed. Thank you.

To Rachelle

ABSTRACT

This thesis describes and evaluates the conversion of a conventional gasoline powered all-terrain vehicle (ATV) to an electric ATV. Preliminary studies are performed to obtain initial power and torque requirements for the vehicle. A detailed simulation model of the mechanical load is written and compared to manufacturer supplied data. The load model is then combined with a comprehensive electronic drive and motor simulation using an electromagnetic transient simulation program (PSCAD). A prototype of the vehicle is constructed by selecting the main components, an electric traction motor, batteries and a custom motor drive, using the simulation results. The results of both the simulation and prototypes are compared and evaluated.

Table of Contents

LIST OF FIGURES

LIST OF TABLES

1 INTRODUCTION

1.1 Automobiles

Over the last 100 years Canadian society has become largely dependent on automobiles for our everyday living. We rely on heavy trucks for transporting our food and goods from other parts of the country and the USA. Light automobiles are heavily used for commuting between work and home. There are approximately 18.6 million vehicles on Canadian roads; these on-road vehicles travelled 315.3 billion kilometres and consumed 39.5 billion litres of gasoline and diesel in 2005 [1]. The consumption of this fuel accounts for 35 percent of the country's greenhouse gas (GHG) emissions [1]. To help reduce the GHG emissions from the automobile sector many different alternatives have been studied, of these options electrifying and hybridizing the drive trains are available options.

1.2 Electric and Hybrid-Electric Power Trains

The electrification of a power train allows for an increase in the overall drive train efficiency, as electrical systems are much more efficient that internal combustion engines (ICEs). A purely electrical drive train is limited only by the capabilities of the energy storage [2]. Current battery technologies lack the amount of energy storage capacity to compare with energy dense carbon based fuels. A synergistic work around for this problem is to combine the energy efficiency of an electrical drive train with the high energy storage capabilities of an ICE through hybridization.

Hybrids are available in essentially two different variants. The first is a series hybrid in which the wheels are driven by the electrical motor and the ICE drives a generator to convert the mechanical energy to electrical energy. The second type of hybrid is a parallel hybrid. A parallel hybrid consists of both an electric drive train and mechanical drive train that are both connected to the wheels of the vehicle. A combined version of both hybrid topologies can also be used and is sometimes referred to as a complex hybrid [4]. The benefit of the hybridization is that the electric drive train can be optimized to operate so that the ICE can run at its peak efficiency, i.e. the ICE shuts down when stopped or coasting. The electric motor can also supply extra torque for acceleration, thus allowing for the installation of a smaller gasoline engine.

1.3 All-Terrain Vehicles (ATVs)

Automobiles are primarily used for on-road travel. A newer segment of small vehicle that is popular in North America is the all-terrain vehicle. The first commercial all-terrain vehicle was the ATC90 introduced by the Honda Motor Company in 1970 [5]. This vehicle was a simple 3 wheeled vehicle with a small 90 cc ICE. The vehicle was originally intended to be used for recreational purposes. The continued development of the three-wheeled vehicles eventually evolved into the four wheel vehicles we are familiar with today. While still used for recreation, the high performance and agile vehicles are used in many application including farming, forestry, natural resource exploration, law enforcement and peacekeeping.

Just as with automobiles, ATVs are powered by inefficient ICEs and thus generate GHG emissions, pollution and noise. ATVs have a very different use than on road vehicles, they travel shorter distances usually at a much slower speed than automobiles

and spend lots of time idling. These conditions make the vehicles ideal to electrify and potentially hybridize to greatly increase their overall efficiency.

1.4 Motivation

As indicated above, many uses of ATVs, such as farm use or resource exploration, involve frequent short trips with lots of stopping. Plenty of stopping amounts to excessively wasteful engine idling and pointless emissions. The off road capabilities allow them to be driven in environmentally sensitive areas where the impact of the emissions or a potential gasoline or oil leak may be substantial. The possibility of reducing the environmental impact of the small vehicle without sacrificing the vehicles high performance is a reasonable target.

1.5 Problem Definition

The goal of this work is to design an electric drive train for an ATV. The selection of components and topology will be such that it will have consistent performance as the conventional gasoline powered ATV. The final design should afford the user the same control and usability as a conventional ATV. The drive train should also allow hybridization to take place in the future.

The components selected for the drive train should not increase the weight of the vehicle and requiring the fewest frame modifications possible. The components will be selected based on existing ATV performance and simulation, endeavouring to match the performance characteristics as close as possible. PSCAD will be used to perform the design and optimization of the electric control system. PSCAD is an electromagnetic transient simulation software for power system simulation that is primarily used in the power system industry. It gives users the ability to write custom simulation modules that

can then be interfaced with the existing library models. This project will exploit that capability and a custom model of the ATV mechanical load will be written.

PSCAD is not primarily used in the design of electric vehicles. Therefore, the second phase of the project is to undertake a prototype implementation of the simulation based design to verify the results of the PSCAD simulation to those of the prototype.

1.6 The Polaris Sportsman 500 ATV

To simplify the mechanical portions of the electric ATV project, a commercially available ATV has been selected as the platform for the electric ATV. Polaris Industries of Minnesota has supplied a Sportsman 500 frame shown in Figure 1.1. The conventional ATV specifications are shown in Table 1.1. The mechanical vehicle model will be developed to match the conventional ATV.

Table 1.1 - Polaris Sportsman 500 specification

Characteristic	Specification
Engine	499 cc, single-cylinder, liquid cooled
Transmission	Fixed gear transmission with variable speed clutch
Vehicle Weight	324.3 kg
Length/Width/Height	210.8 cm/121.9 cm/ 121.9 cm

Figure 1.1 - The Polaris Sportsman 500

1.7 Outline of Thesis

The design of an electric vehicle requires the understanding of the mechanical and electrical systems involved as well as the individual components that are required. Chapter 2 of the thesis covers the general background of different topologies of electric and hybrid electric vehicles as well as the components that can be used to build such vehicles, some of their associated advantages and disadvantages will be discussed.

Chapter 3 covers the design and simulation stage. The initial discussion focuses on preliminary calculations to determine the performance requirements. The model development of the mechanical system is covered in detail as well as the simulation of the electrical machine, power electronic motor drive and control approach.

Chapter 4 presents the electric ATV prototype. In this chapter, the features included in the design, to afford the user the same control as a conventional ATV, are discussed.

Chapter 5 presents the comparison of the PSCAD simulation results to the prototype results, describing any inconsistencies and difference between the results. Finally, chapter 6 concludes the thesis by presenting the contributions and recommendations for future work.

2 BACKGROUND

2.1 Benefits of Electric and Hybrid Vehicles

Decreased fuel consumption, or the elimination of fossil fuel all together can be seen as the biggest overall benefit of HEVs and EVs. This reduction or elimination of combustion also potentially reduces the overall GHG emissions and pollution. EVs have the ability to provide emission free urban transportation. If the power plants that generate the electricity are taken into consideration, the overall emissions are still greatly reduced [6]. EVs also greatly reduce the level of noise pollution.

The design of electric vehicles involves the integration of mechanical and electrical systems and, as such, a thorough understanding of the components that make up the vehicles is important. The following sections briefly discuss an overview of the different vehicle topologies as well as the components that form the systems of the vehicles.

2.2 Electric and Hybrid Vehicle Topologies

2.2.1 Electric Vehicles

EV's come in many forms using many different technologies. The individual components and different technologies will be described in a later section. EVs are mainly comprised of three different blocks: (i) an energy storage device, (ii) an electric drive and (iii) an electric motor. There may also be a mechanical transmission that will link the electric motor to the drive wheels of the vehicle. The electric drive has the job of controlling the flow of energy through to the traction motor. A typical EV drive train can

be seen in Figure 2.1. The drive may also have the capability of controlling the flow of energy from the drive tires through to the energy storage device. This is known as regenerative braking [2].

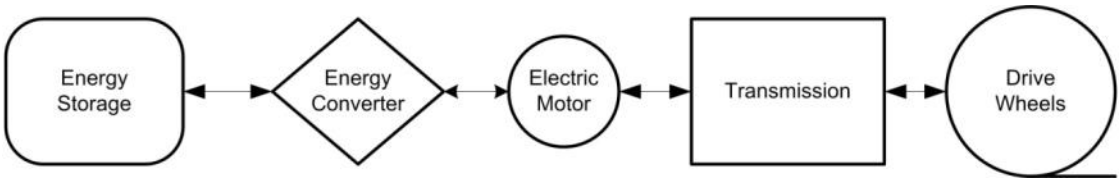

Figure 2.1 - Typical electrical vehicle topology

2.2.2 Hybrid Electric Vehicles

HEVs can be described primarily by two different topologies: series and parallel. The two technologies may be combined, forming a complex hybrid. The level of hybridization is determined by the available electrical power. The more electrical power the higher the level of hybridization the vehicle is said to have [7]. Hybridization also allows for a smaller ICE to be used when compared to a similarly performing non-hybrid vehicle.

2.2.2.1 Series Hybrid

A series hybrid was originally used to extend the range of existing electrical vehicles [10]. As can be seen in Figure 2.2, a series hybrid is essentially a vehicle that has an electric drive train similar to an electric vehicle. It also has an ICE connected to a generator that can supply power through to the traction motor or to the energy storage device or both. The benefit of this configuration is that the ICE can be tuned to run at its most efficient operating point and only when it is required. This completely eliminates

wasteful idling. The energy converter controls the flow of energy between the generator, energy storage and traction motor. The energy converter may also allow for regenerative braking further increasing the overall efficiency of the vehicle.

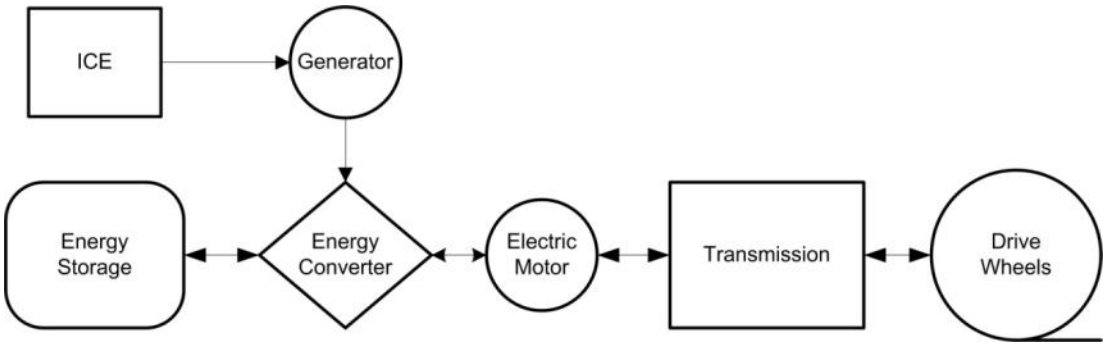

Figure 2.2 - A series hybrid electric vehicle topology

2.2.2.2 Parallel Hybrid

A parallel hybrid, demonstrated in Figure 2.3, has two drive trains connected to a common transmission [2], [4]. The first drive train is similar to that found in a conventional gasoline powered vehicle where the ICE is connected directly to the transmission. The second drive train is the electrical energy storage and electric traction motor connected to the transmission. The transmission controls the distribution of the energy in multiple ways: (i) Uses both drive trains to power the wheels of the vehicle increasing the performance. (ii) Uses the ICE to drive the wheels and send a portion of the ICE's power to run the motor as a generator and recharge the batteries. (iii) Uses the power from the wheels when braking to turn the motor, again as a generator and recharge the batteries. The ICE in a parallel hybrid cannot typically be controlled to operate at its

peak efficiency all the time, although it can be shut down when stopped or coasting to eliminate wasteful idling.

Different combinations of series and hybrid drive trains can be placed together in the same vehicle along with additional motors, generators and additional energy storage and control devices. These complex hybrids essentially offer more sophisticated control of the energy flows at the expense of more complex hardware schemes. A more recent introduction is the plug-in-hybrid electric vehicle (PHEV), in which a large energy storage device is added to an HEV. This PHEV can then travel for a limited range in an all-electric mode and then recharge from the electricity grid.

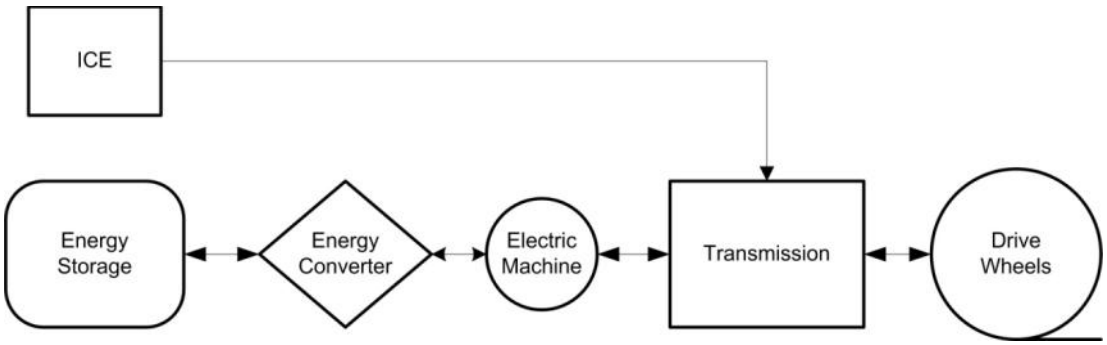

Figure 2.3 - A parallel hybrid electric vehicle drive train

2.3 Drive Train Components

As can be seen from the descriptions of electric and hybrid vehicles above, there are essentially 5 different types of components that may be found in a drive train. These items are: (i) an internal combustion engine, (ii) an electric motor/generator, (iii) a mechanical power converter/splitter, (iv) electrical energy storage and (v) electrical

power converter. Each of these components as well as the different options are described next.

2.3.1 Internal Combustion Engine

The ICE is found only in HEVs. The ICE turns chemical energy in the form of gasoline or diesel fuel into mechanical energy through combustion [2]. As described above it can deliver mechanical torque directly to the drive wheels of the vehicle through a set of gears or transmission. It can also deliver all of the mechanical energy to a generator which converts it into electrical energy. The more sophisticated hybrid vehicles allow the torque to be split, to generate electrical energy and drive the vehicle at the same time.

2.3.2 Electric Motor/Generator

The electric motor has the primary purpose of supplying mechanical torque to the drive wheels of the automobile. The secondary function of the motor is to generate electric energy through a generation mode by accepting mechanical torque from the drive wheels. There are different types of electrical motors that can be used for EVs and HEVs.

DC machines are the simplest motors to control as the source of electrical energy is already stored in a dc state [8]. The dc machine has many mechanical components such as commutator and brushes. These added mechanical components add to higher maintenance requirements over ac machines. The highest efficiency point of dc machines is near the maximum rated speed.

AC or alternating current machines offer great efficiency over a broad range of speeds; however they require more complex and sophisticated control systems and drives

than their dc counterparts. There are multiple variants of ac machines available, including induction, synchronous and permanent magnet. Induction and permanent magnet machines can be controlled with a similar converter whereas a synchronous machine requires an added dc excitation system to create a magnetic field on the rotor.

2.3.3 Electrical Power Converter

The electrical power converters or drives to control dc machines are much simpler than ac machines [9]. They are required only to generate a varying dc voltage. Depending on the dc source, a converter may be required to either step up or step down the voltage or a converter to perform both. A dc/dc converter creates a variable dc voltage by controlling the time the full dc voltage is connected to the load through power electronic switches. These switches are turned on and off at high frequencies effectively chopping the voltage. By adjusting the period of time the switch is on, or the duty cycle, one can adjust the average voltage seen by load. Figure 2.4 depicts the resultant steady state waveforms of a dc/dc converter driving an inductive load with a resistance of 10Ω. The switching frequency is 10kHz and the duty cycle of 75% gives an average voltage of 75V and a load current of 7.5A. A small ripple is observed on the current due to the periodic switching of the voltage.

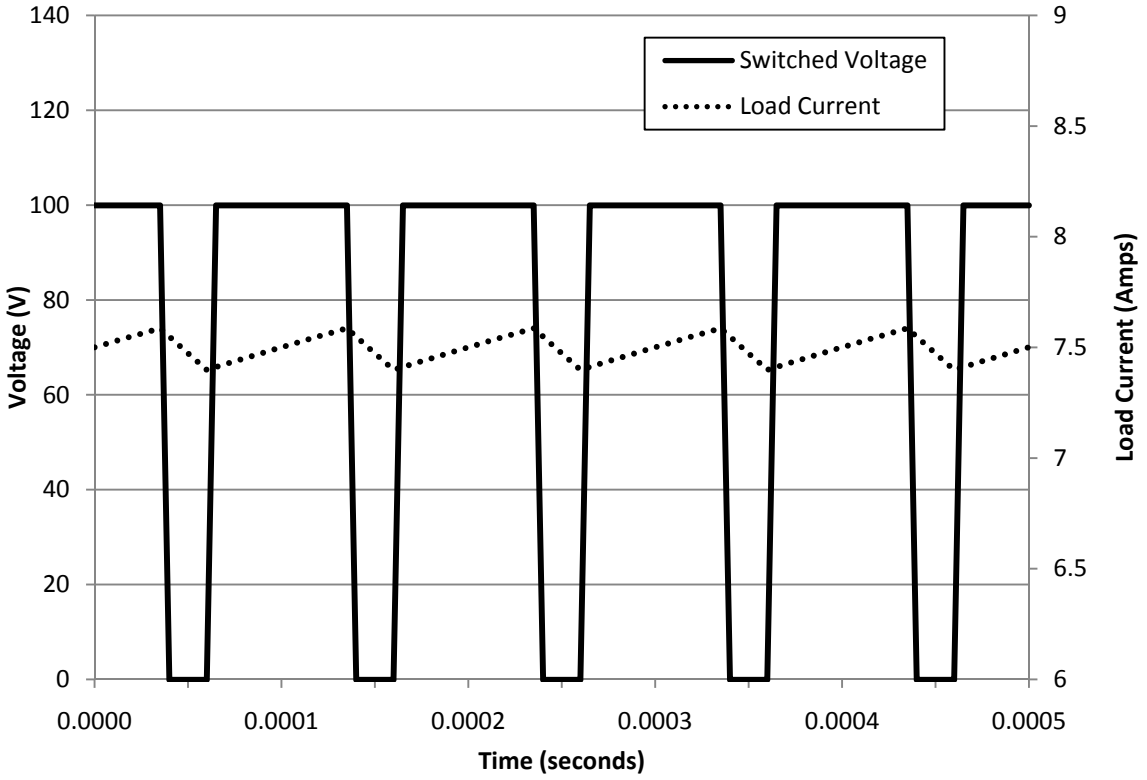

Figure 2.4 - Voltage and current of a dc/dc converter

Ac machine drives require a means of controlling the individual phase voltages in a sinusoidal fashion. If the ac machine is a multi-phase machine, a set of switches are required for each phase. Depending on the number of switching levels that are used, the set number of switches the converter requires varies: i.e. a 2 level converter requires 2 switches per phase and a three level converter requires 4 switches per phase. An ac drive works in a similar fashion as a dc/dc converter. The main difference is that the duty cycles of the switches are varied in such a way as to shape the load current into a sinusoidal waveform. This waveform's magnitude and period can be adjusted by controlling the duty cycles. Figure 2.5 shows the output of a two-level dc/ac inverter through one cycle of ac output.

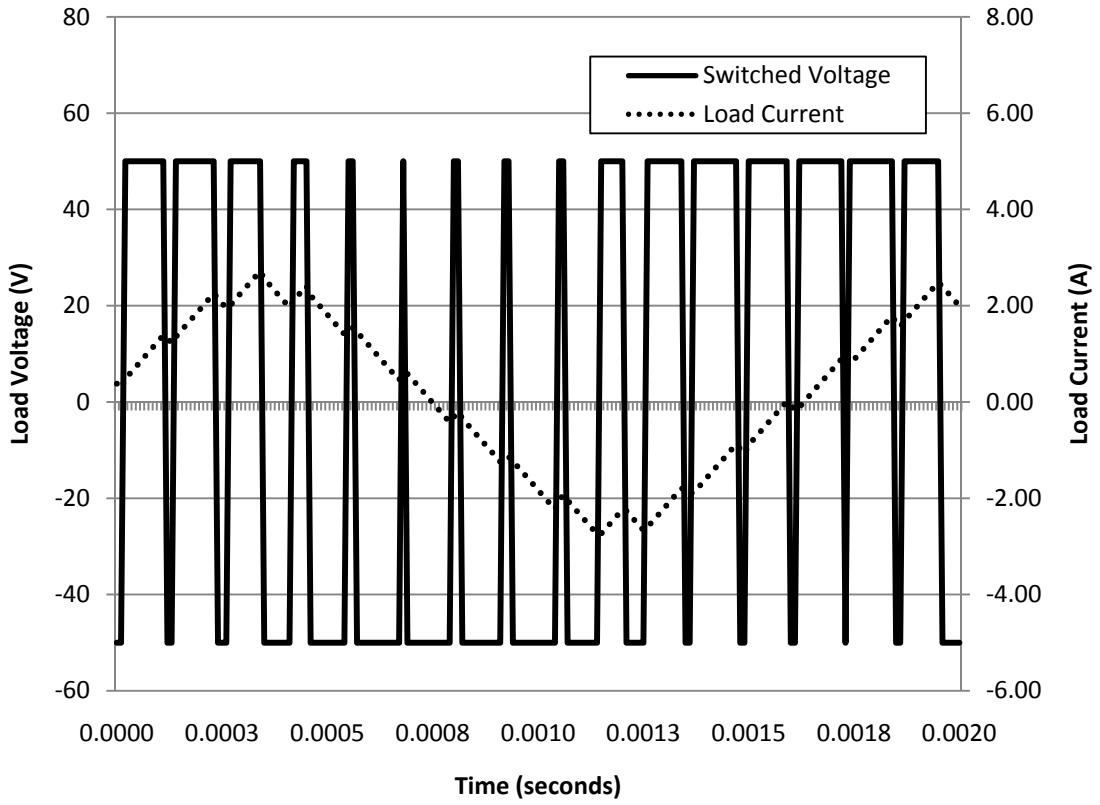

Figure 2.5 - Voltage and current waveforms of a dc to ac inverter

2.3.4 Mechanical Power Converter/Splitter

In an HEV, the electric traction motor may be called upon to supply additional torque when accelerating the vehicle. This additional torque will need to be added to the torque being supplied by the ICE. A transmission between the drive wheels and the sources of torque must have the capabilities to: (i) combine the torque inputs to the wheels; (ii) depending on the need of the vehicle, multiply or divide the input torque to the required output level; (ii) divide a single input torque to multiple outputs, such as torque from the ICE being used to drive the wheels and turn the generator to store energy [7], [10].

Depending on the number of torque sources, the transmission may be required to distribute and convert multiple inputs to multiple outputs. An example of this type is the transmission that can be found in the Toyota Prius [11].

The electric machine in an EV may also be coupled to the drive wheels by the means of a transmission. A transmission coupling allows for an electric machine with a small output torque to be used, as the transmission will act as a torque multiplier at low speed. It should be noted that added gearing and transmissions decrease the overall efficiency of the vehicle.

One way to increase the efficiency of the electric vehicle is to select a machine that has the torque capabilities to bypass the transmission and directly drive the differential of the vehicle. Another approach to increase the efficiency is to eliminate the mechanical differential and place a motor on each wheel. The function of the differential can be replaced by the motor controllers.

2.3.5 Electrical Energy Storage

The primary means of energy storage for existing ICE powered vehicles is gasoline. Gasoline has a tremendous energy density [2]. A benefit of gasoline is the speed and ease at which the vehicle can be refuelled, or "recharged". There are of course many disadvantages to gasoline such as, the current conversion efficiency of the ICE. An ICE converts an average of 20% of the chemical energy of gasoline to mechanical energy with the remaining energy converted to heat [2]. The environmental and health effects of the waste products produced by the combustion of gasoline are also disadvantages.

2.3.5.1 Fuel Cell

Hydrogen in either a compressed or liquid form can be converted into electrical energy by a hydrogen fuel cell through catalysis. Fuel cells are considered to be the most promising but least developed technology for automobile propulsion. A simple way to describe a fuel cell is as an easily refillable electric battery. Although fuel cells do not store energy, they generate the energy by combining the hydrogen with oxygen. The technology is promising as there are no direct GHG emissions or by-products. The result of the hydrogen-oxygen catalysis is pure water. Fuel cells are currently an expensive technology with no commercially available system appropriate for the ATV. As fuel cells will not play a role in the ATV project, the details for this report have been limited.

2.3.5.2 Ultra-Capacitors

Electrical energy storage can be found in the form of ultra capacitors. Ultra capacitors are electrochemical capacitors that can support a large power output and input for short periods of time due to their limited energy density [3]. Their large power density makes them very useful for hybrid vehicles to provide the rapid amounts of power required to accelerate vehicles and absorb the large amount of energy during regenerative braking. The small energy density of ultra-capacitors limits their application in electric vehicles and thus they will not be used on the electric ATV.

2.3.5.3 Batteries

The most recognized form of electrical energy storage is in the form of batteries. Batteries store electrical energy through conversion to chemical energy. Battery research is very active and new promising battery technologies are continually being announced. For the purpose of this report there are three types of prominent batteries technologies

worth explaining: (i) lead-acid, nickel metal-hydride (Ni-MH) and lithium-ion (Li-Ion) [4].

Lead-acid batteries have been around since the earliest days of electric vehicles. The energy density of lead-acid batteries is often used as a base when comparing different battery technologies. Lead acid batteries can supply and absorb a large current. As the energy density of lead acid is not very high, the mass and volume of the batteries required to store a functional amount of energy is a problem. Also, lead acid batteries do not have a long deep cycle life.

Ni-mH batteries can have up to three times the energy density of lead-acid batteries per unit volume and weight. The batteries can supply a large current. However, when charging the batteries only a fraction of the supply current can be applied. The limitation on the charge current results in an extended re-charge period. Ni-mH batteries have a much better life when deep cycle discharged when compared to lead-acid.

Li-Ion batteries have approximately four to five times the energy density of lead acid batteries for the same unit and weight. The volume of Li-Ion batteries is also much smaller than their lead-acid counterparts. Similar to Ni-mH batteries, they can supply a large current but can only absorb a fraction of this current when being charged. Altair Nanotechnologies has recently introduced a highly stable lithium technology capable of accepting a large current. Their 35kW battery pack can be recharged in 10 minutes [12].

The discharge characteristic of a Li-Ion battery is practically a constant voltage. This is in general a desirable characteristic to have for a battery, but adds complexity when trying to monitor the state-of-charge (SOC). This constant discharge characteristic brings about the requirement of a battery management system to monitor the energy in and the

energy out of the battery. This management technology enables excellent deep cycle discharge life and can monitor additional items, such as the temperature, to extend their service life. Li-Ion batteries are currently extremely expensive when compared to other battery types [13]. Table 2.1 is a comparison of the different battery technologies [7], [14].

Table 2.1 - Comparison of EV batteries at "deep cycle" condition

High Energy Design in Deep Cycle Applications	**(Units)**	**Lead Acid**	**Nickel Metal Hydride**	**Lithium-Ion**
Energy density	**(Wh/Kg)**	35	70	>90
Power density	**(W/Kg)**	150	200	600
Life time (number of cycles)	**At 80% depth of charge**	125	3,000	2,500
Cost level	**USD/kWh**	150	450	500

Now that we have seen the different vehicle topologies and had a brief overview of the components that make up EVs let us proceed to the design philosophy and component selection to model the electric ATV.

3 DESIGN AND SIMULATION

3.1 Design Philosophy

As mentioned in chapter one, the electric ATV's design shall be integrated into an existing Polaris Sportsman ATV frame. The existing mechanical gear case and drive axles (both the front and rear) shall be used as the primary means of power transfer to the wheels; the suspension components shall also be used. The combination of these requirements defines an overall approach to the design. Integrating EV components into an existing frame requires that the new drive components fit into the space allowed in the existing vehicle, while trying to maintain a similar mass distribution as the gasoline power system. The existing ATV has pre-defined and well known operating characteristics such as acceleration and top speed. It is these characteristics that will form the base on which the design of the electric ATV shall start.

The preliminary design shall be first discussed, including a description of the existing ATV's function and systems. Using the results from the preliminary design, the selection of the basic component ratings is presented, leading to the detailed design of the mechanical and electrical simulation models designed for use in PSCAD. The chapter will conclude with a description of the tuning and optimization of the complete simulation case.

Before proceeding with the design details of the ATV it should be noted that the vehicle is being designed with only an electric drive train. The design of a prototype

electric vehicle focusing on the optimized electric drive train will act as a proof of concept that could be further extended by adding an ICE, transforming the vehicle into a plug-in series hybrid.

3.2 Preliminary Design

To begin the preliminary design, the existing ATV and the modification of the vehicle must be described. The gasoline powered ATV has an ICE that is connected to a fixed ratio gearbox by means of a proprietary continuously variable transmission (CVT). The CVT allowed a more efficient torque-speed characteristic of the ICE to be achieved while at the same time affording the user the ease of not having to shift gears while driving. The fixed ratio gearcase incorporates the ability to transmit power to either the rear axle only or to both front and rear axle when the all-wheel drive (AWD) option is engaged. The rear axle is incorporated directly into the fixed ratio transmission. Figure 3.1 gives a general overview of the placement and components of the existing ICE based power train.

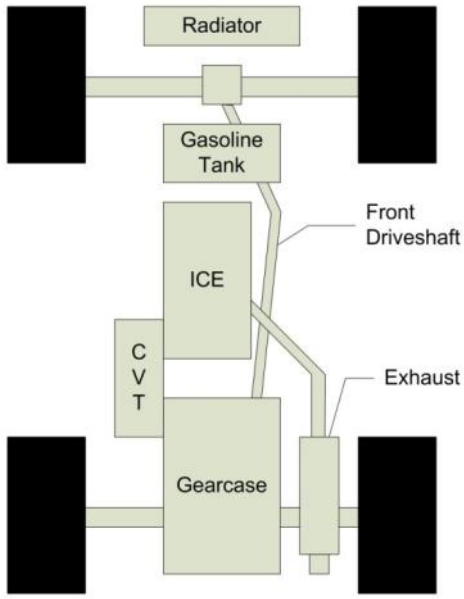

Figure 3.1 - Overview of the mechanical system of the existing ATV

To electrify the ATV, the internal combustion engine and all of its associated components including the radiator, exhaust system and fuel storage tank are removed. The CVT is removed as the torque-speed characteristics of electric machines do not require the dynamic gear range. For reasons mentioned previously the gearcase is not removed as it will simplify the mechanical design of the prototype. Drive train modifications are only being made from the point of connection to the gear case forward. Figure 3.2 is a generalization of the electric drive train to be placed on the ATV frame which includes batteries for energy storage, an electric machine, a power converter and mechanical coupling from the motor to the gearcase.

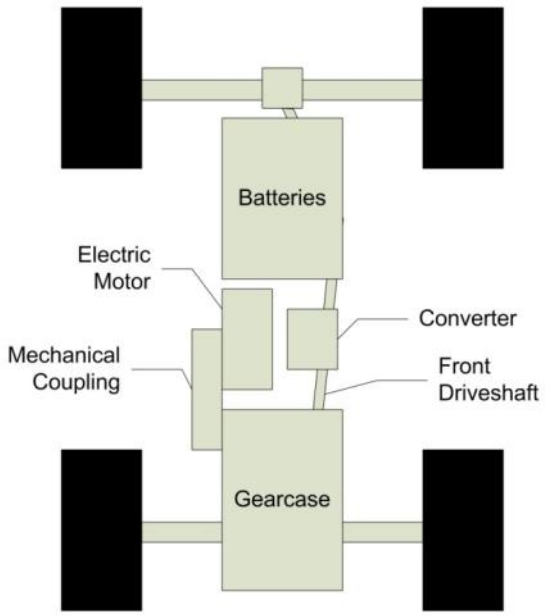

Figure 3.2 - Overview of the electrical conversion of the ATV

To fit the new components into the existing chassis presents two challenges, namely (i) fit a powerful electric machine and energy storage system in existing spaces and (ii) minimizing the number of modifications that will have to be made to the frame. These two challenges have to be met while minimizing the increase in weight over the conventional ATV. The goal of the preliminary design is to allow for the initial selection of electrical components based on general power and energy calculations.

3.2.1 Power, Energy and Torque Requirement Calculations

Analysis of the performance of the ATV will use a straight line, or longitudinal model. This model will allow for the determination of the acceleration performance, the top speed and the gradeability. Gradeability is a measure of the performance of a vehicle while climbing a desired grade angle. Parameters that will not be considered are the cornering capabilities and the latitudinal roll of the body. These parameters are not

considered since the suspension of the vehicle is not being modified and the load distribution of the new components is to be similar to the conventional. For most on-road vehicles these longitudinal parameters are sufficient to determine a good measure of the overall longitudinal performance [16].

There are multiple forces acting on a vehicle in motion. For the purpose of calculating the minimum power and energy requirements, only two forces are important: the aerodynamic drag force and the rolling resistance force as described by equations 3.1 and 3.2 respectively. Where F (N) is the force, ρ (kg/m^2) is the density of air, C_d is the aerodynamic drag coefficient, A (m^2) is the frontal cross-sectional area of the vehicle, v (km/hr) is the velocity of the vehicle, v_0 (km/hr) is the velocity of the head wind, μ is the rolling resistance coefficient, m (kg) is the mass of the vehicle and α (degrees) is the angle of inclination.

$$F_{aero} = 0.0386 \cdot \rho C_d A (v + v_0)^2 \tag{3.1}$$

$$F_r = \mu m g \cdot cos\alpha \tag{3.2}$$

To determine the minimum power requirements no wind or road grade is assumed. An added benefit of modifying an existing commercial vehicle is that the aerodynamic drag and rolling resistance coefficients and the vehicles general characteristics are known. These can be found in Table 3.1.

Table 3.1 - Polaris Sportsman 500 specification

Characteristic	Specification
μ- Rolling Resistance Coefficient	0.045
C_d - Coefficient of Drag	0.72
A - Frontal Area	1.75 m^2
$m -$ Vehicle Mass (75 kg for rider)	400 kg
r_w effective wheel radius	0.3175 m

The minimum power requirements are determined by calculating the aerodynamic drag force and the rolling resistance force acting on the vehicle at different velocities. The force is then and converted to instantaneous power using equation 3.3 where P (kW) is the instantaneous power requirement.

$$P = \frac{v}{3600} F \tag{3.3}$$

For the power calculations 80 km/hr is used as the top speed as the existing commercial ATV has a top speed of approximately this value. The results of the power calculations are shown in Figure 3.3. The overall power requirement to maintain a velocity of 80 km/hr on a level grade with no wind is 9.5 kW. This value does not account for the losses accumulated in the drive train, and thus a margin must be added to account for these losses.

The power numbers could also be used to calculate approximate energy storage requirements. If we select an average speed of the vehicle to be 50 km/hr and we would like to have a range of 50 km, we take the power requirement at 50 km/hr and multiply it by the time required to travel 50 km, which in this case is one hour. This would require approximately 3 kWh of energy storage. This number is not a true representation of the energy requirement as it does not account for the energy used in accelerating the vehicle

up to the desired speed, as well the multiple number of times that the vehicle will likely be accelerated. As mentioned above, the drive train losses are not accounted for in these calculations. The number does give a good indication of an absolute minimum amount for an energy storage capacity.

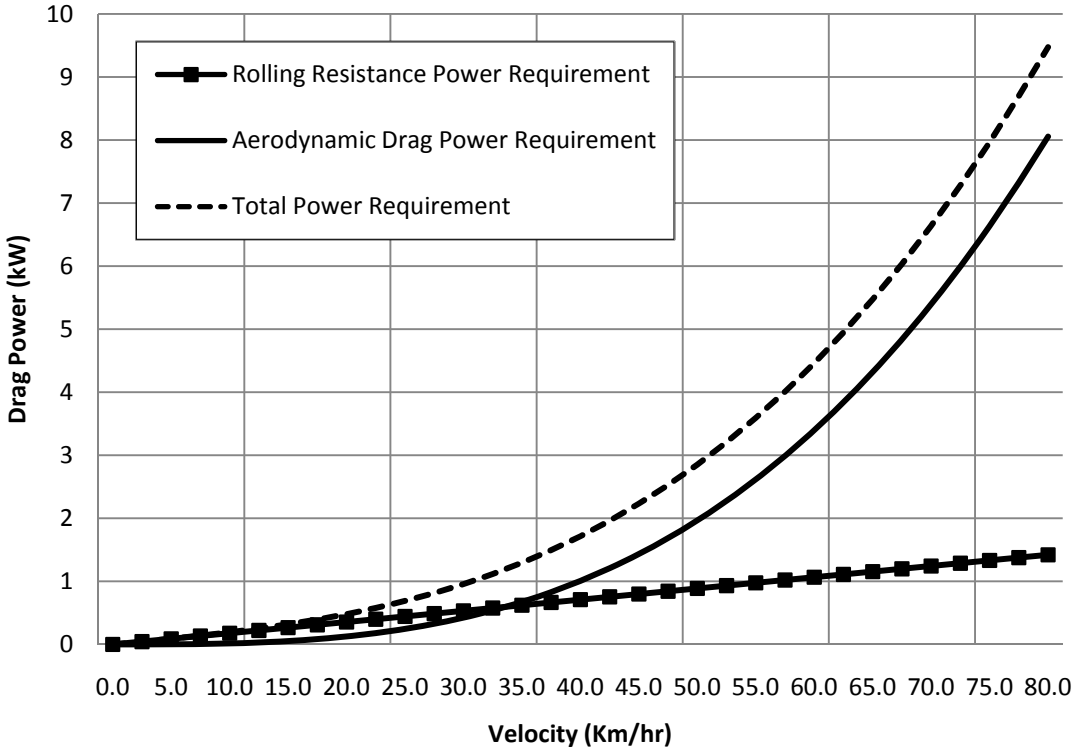

Figure 3.3 - Minimum power requirements of the ATV

An electric motor generates mechanical power in the form of a rotational torque. To better select an electric machine, the torque requirements of the vehicle can be calculated from the power curves using equation 3.4. Where T (Nm) is the torque measured at the wheel axle and r_w (m) is the effective wheel radius. When the speed is zero, there is an singularity that produces a 0/0 case, if the limit is taken as the speed approaches zero a starting torque of 20.4 Nm is determined. This indicates that there is an amount of torque

that must be overcome to move the vehicle. The load torque curve is demonstrated in Figure 3.4.

$$T = \frac{3600 \cdot r_w}{v} P \tag{3.4}$$

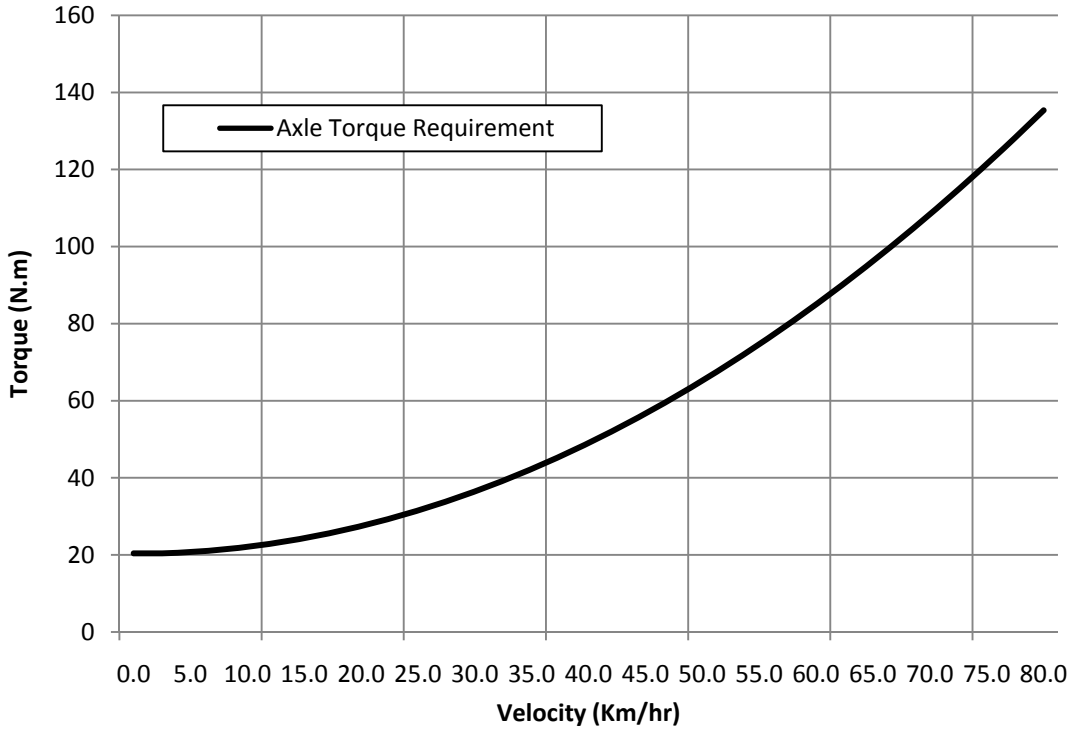

Figure 3.4 - Minimum axle torque requirement

3.3 Basic Component Selection

The calculated minimum values for the power requirement and the energy storage can be used to determine the selection of the electric machine and the main battery. The selected motor will add further restriction to the battery selection in terms of voltage and current requirements. Consequently, a motor selection is completed first, followed by the battery.

3.3.1 Electric Machine Selection

Using 80 km/hr as a top speed for the vehicle, the minimum power required of the selected electric machine, from Figure 3.4, is 9.5 kW. The electrical machine will deliver the power through the gearcase which reduces the speed of rotation but acts as a torque multiplier. This reduces the axle torque by the gearcase gearing ratio which becomes the motor torque requirement. The gearcase ratios are given in Table 3.2. The high gear will require a minimum of 12.66 Nm, ignoring the mechanical losses. This significantly smaller torque will have to be delivered at a speed that is the gear ratio times greater than the speed of the wheels.

Table 3.2 - Polaris gearcase ratios

Gear Selected	Ratio
Park	N/A
Reverse	16:1
Neutral	N/A
Low	24:1
High	10.66:1

The wheel speed can be calculated roughly by equation 3.4, where N_e (rpm) is the electrical speed of the machine, v (km/hr) is the peak velocity of the vehicle, d_w (m/revolution) is the distance travelled per wheel rotation and ζ_g is the gearcase ratio. The constant in the equation is used to convert the velocity from km/hr to metres per minute. Using equation 3.5 and the high gear ratio of the gearcase the required speed of the machine to achieve 80 km/hr is 7105 rpm.

$$N_e = 0.06\frac{v}{d_w}\zeta_g \tag{3.5}$$

As discussed in the background section, there are many options available to select for the traction machine of the electrical ATV. The primary constraints in selecting the electric machine are not only the power, torque and speed requirements, but also the very restrictive size and weight requirements of the small ATV frame. The size and weight restriction eliminate induction and synchronous machines as their power rating per kilogram of mass is relatively low. A permanent magnet synchronous machine, manufactured by PERM, has been selected as the starting point for machine selection because it is a relatively compact machine for its power rating, its efficiency is greater than 90% and it has a very high power density. The gearcase ratio from Table 3.2 is used to convert the peak axle torque requirement to an electrical motor shaft torque. After the conversion, as shown in Table 3.3, the machine exceeds the power and torque requirements which will allow room for the mechanical losses of the gear case. The speed rating has not been met which will reduce the top speed, or a mechanical coupling that will adjust the ratio will have to be selected later. A summary of the electrical machine requirements and the PERM PMS-150 machine data from the motor data sheet is shown in Table 3.3.

Table 3.3 - Summary of electric machine parameters and requirements

Characteristic	Project Requirement	PERM PMS-150 Specs
Power Rating	9.5 kW	13 kW
Electrical Torque	12.66 Nm	27.5 Nm
Electrical Speed	7105 rpm	4500 rpm
Efficiency	-	94 %
Mass	-	33.0 kg
Power Density	-	0.4 kW/kg
Rated Line Voltage	-	66.5 $V_{ac\text{-}rms}$
Rated Current	-	151 A_{rms}

3.3.2 Battery Voltage Selection

Having selected a base motor, a battery can now be selected. The voltage level of the battery has to be selected so the inverted ac voltage will match the rated voltage of the machine. Using sinusoidal PWM techniques without going into saturation region to generate the ac voltage waveforms we can achieve a peak ac voltage equal to the dc voltage of the battery. Converting the 66.5 V_{rms} of the motor to a peak value gives 94 V, therefore a battery pack with rating of at least 94 volts is required. The energy storage capacity of the batteries is not crucial as the range of the prototype vehicle can be extended at a later date by adding further battery capacity. The size and weight restriction again limit the battery technologies. As mentioned in the background section Li-ion batteries have the highest energy density of the main battery technologies considered. Valence technologies of the USA offers Li-ion battery packs with 19.2 V ratings and an energy capacity of 1.25 kWh per battery pack. By creating a series string of 5 of the battery packs 96 volts is achieved with a total energy capacity of 6.25 kWh. This meets the motor voltage requirement and supplies sufficient energy storage for testing. Further details on the batteries will be discussed in the next chapter.

3.4 Simulation Model Design

Having selected the basic requirements for an electric machine and a battery voltage level, simulation models of the system can be developed. The models are used to show that the minimum requirements can be met, as well as determine further requirements for the components, such as the current and power ratings of the required power electronic converter. The electric ATV's power controller fundamentally consists of fast switching high-power static switches. This fast switching generates high frequency transients that

propagate through the electrical and mechanical systems having effects on the acceleration, speed and torque profiles of the vehicle. As mentioned in chapter 1, the models developed for simulation of the overall vehicle are designed for PSCAD, a primarily electrical based modeling program. PSCAD also has the capabilities to design custom components which can model any system capable of being described mathematically, including the mechanical part of the system. The primary advantage of performing the simulation stage of the vehicle before implementation is the ability to try different component ratings, or components reducing the time and money spent during the prototyping stage.

3.4.1 Mechanical ATV Model

A model of the mechanical system of the ATV is developed as a custom component in PSCAD to match the mechanical characteristics of the commercially available Polaris ATV. The model acquires as an input the electric motors current torque output. It then calculates the effect of this torque on the vehicle, taking into consideration the aerodynamic drag, rolling resistance, gradient force, mechanical losses and the slipping of the wheels on the terrain. It returns to the motor model the current speed of the gearcase shaft based on the effect of the torque, which could be acceleration, deceleration or no change. The basis of the model is Newton's second law of motion.

$$F_{net} = ma = m\frac{dv}{dt} \tag{3.6}$$

In equation 3.6, m (kg) is the mass of the vehicle, v (m/s) is the velocity of the vehicle and F_{net}(N) is the net force applied after the external forces acting on the vehicle

are subtracted. The electrical motor torque is converted from torque to a tractive force (F_{trac}) using equation 3.7. Where T_e (Nm) is the electrical motor torque, ζ_G is the gearcase ratio, η_G is the efficiency of the mechanical gearing, and r_w (m) is the wheel radius.

$$F_{trac} = \frac{T_e \zeta_G \eta_G}{r_w} \tag{3.7}$$

The external forces to be subtracted from F_{trac} include the aerodynamic drag force (F_{aero}), rolling resistance force (F_{rr}), and road grade or inclination force (F_{grad}) which are described by equations 3.8, 3.9 and 3.10 respectively. Where ρ (kg/m^3) is the density of air, C_d is the aerodynamic drag constant, A (m^2) is the cross-sectional frontal area, v_0 (m/s) is the head wind velocity, μ is the rolling resistance coefficient, g (m/s^2) is the gravitational constant and α the angle of inclination of the terrain. There are two additional features that are accounted for in the model, the maximum tractive effort, including wheel slip, and the AWD traction mode.

$$F_{aero} = \frac{\rho}{2} C_d A (v + v_0)^2 \tag{3.8}$$

$$F_{rr} = \mu m g \cdot cos\alpha \tag{3.9}$$

$$F_{grad} = mg \cdot sin\alpha \tag{3.10}$$

The maximum tractive effort that can be applied to the ground is directly related to the properties of the ground. Different surfaces, such as asphalt and ice will have

different values of friction, which will limit the maximum force that can be applied to accelerate the vehicle without spinning the wheels. The tire revolution per minute (RPM) of a vehicle is dependant only on the total gear ratio and its efficiency [7]. One would assume that the vehicle speed is therefore proportional to the tire RPM. The parameter referred to as wheel slip contributes to losses in the system resulting in a lower than expected speed. The relationship of tire RPM to vehicle speed is defined in equation 3.11 where n_e (rpm) is the electrical motor speed and s is the value of wheel slip, where 0 is no slip at all, and 1 is the tire completely slipping in place resulting in no forward motion at all.

$$V = \frac{2\pi}{60}\frac{n_e r_w}{\zeta_G}(1 - s) \tag{3.11}$$

There is a theoretical maximum tractive force that can be exerted on the tire contact patch on the ground. This is referred to as the normal force of the vehicle and is described by equation 3.12, which is the force upon which gravity is pulling down on the vehicle. Due to properties of the tire and the characteristic of the ground this maximum force can never be achieved. To model the correct maximum tractive force the properties of both the ground (i.e. surface friction) and the tire must be modeled. These two properties are considered by modeling wheel slip.

$$F_n = mg \cdot cos\alpha \tag{3.12}$$

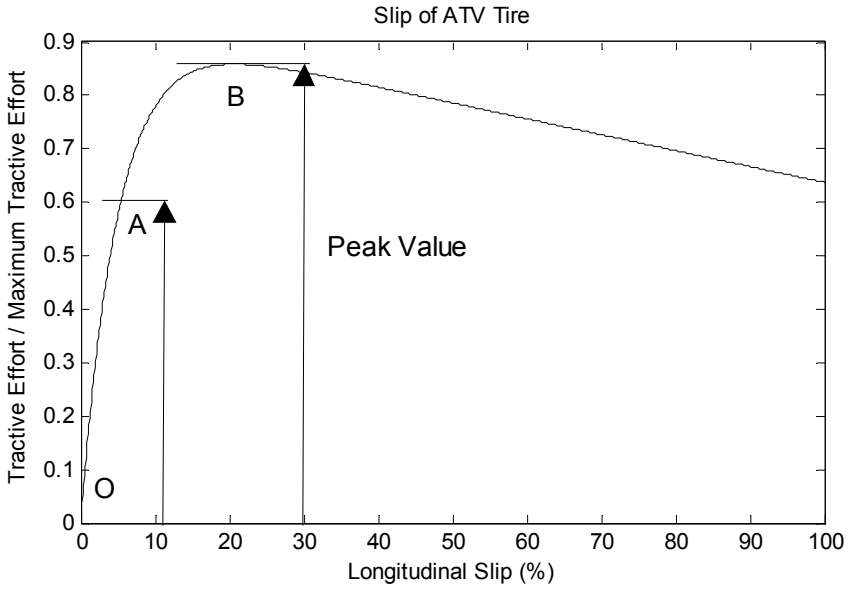

Figure 3.5 - Wheel slip curve for a typical tire

Figure 3.5 shows a typical experimentally derived wheel slip curve as a function of tractive effort. Under steady conditions, the tractive force developed by the tire is proportional to the applied wheel torque. Section OA of the curve corresponds to a linear increase of the tractive effort with wheel slip. This portion of the curve is due to the elastic deformation of the tire tread. As wheel torque is increased beyond this region, there is a non-linear increase in tractive effort with wheel slip, corresponding to section AB. This non-linear increase is due to a gradually larger portion of the tire tread sliding on the ground. According to [15], the maximum tractive force of a pneumatic tire on a hard surface is usually reached of a wheel slip value between 15 and 20%.

The model uses portion OB of a typical wheel curve. The peak value, point B, is adjusted, based on the type of ground selected, using the average values found in

Table 3.4 [16]. The value of slip is calculated using the Newton-Raphson method of successive approximation [17].

Table 3.4 - Average values of tractive effort on various road types

Surface	Peak Values, μ_p	Sliding Values, μ_s
Asphalt and Concrete (dry)	0.8-0.9	0.75
Concrete (wet)	0.8	0.7
Asphalt (wet)	0.5-0.7	0.45-0.6
Gravel	0.6	0.55
Earth Road (dry)	0.68	0.65
Earth Road (wet)	0.55	0.4-0.5
Snow (hard packed)	0.2	0.15
Ice	0.1	0.07

The prototype ATV will have the capabilities to run in a two wheel drive mode where all the power is transferred to the rear axle only, as well as all-wheel drive mode (AWD) in which all the wheels are powered. The AWD mode allows the ATV to accelerate at a faster rate when subjected to different types of surface conditions, a direct result of less wheel slip due to the tractive effort going to all four wheels instead of only two. Taking into account the AWD option allows the user to see the effects of the decrease in wheel slip as well as the effect of the added mechanical losses that are present when torque is delivered to both axles.

3.4.1.1 Mechanical Model Validation

The final version of the mechanical model is a single component within PSCAD as shown in Figure 3.6. The two input connections on the model, found on the left hand side, are used to input the electrical torque from the motor (Nm) and a Boolean input that will select the high or low gear ratio of the gearcase. The outputs of the model, on the right-hand side output the acceleration (m/s^2), the velocity (km/hr) and the electrical speed of the machine in rpm. The vehicle characteristics are input through the parameter input dialogs seen in Figure 3.7.

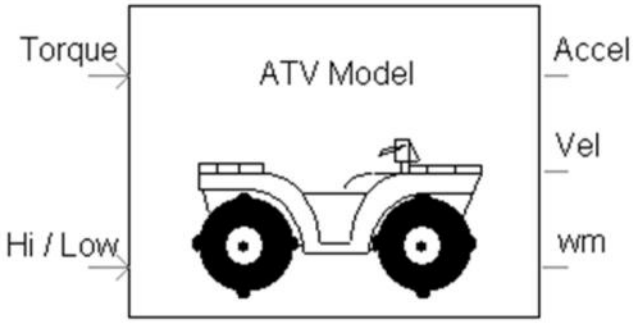

Figure 3.6 - PSCAD ATV model

The input dialog allows for the entry of the parameters required to solve the equations describing the mechanical system. The model allows for the values to be input as external variables that can be modified from the simulation space during the simulation. The name WIND is an example of an external variable that can be used to adjust the wind speed during the simulation. The values listed are those that are used to describe the electrical ATV prototype.

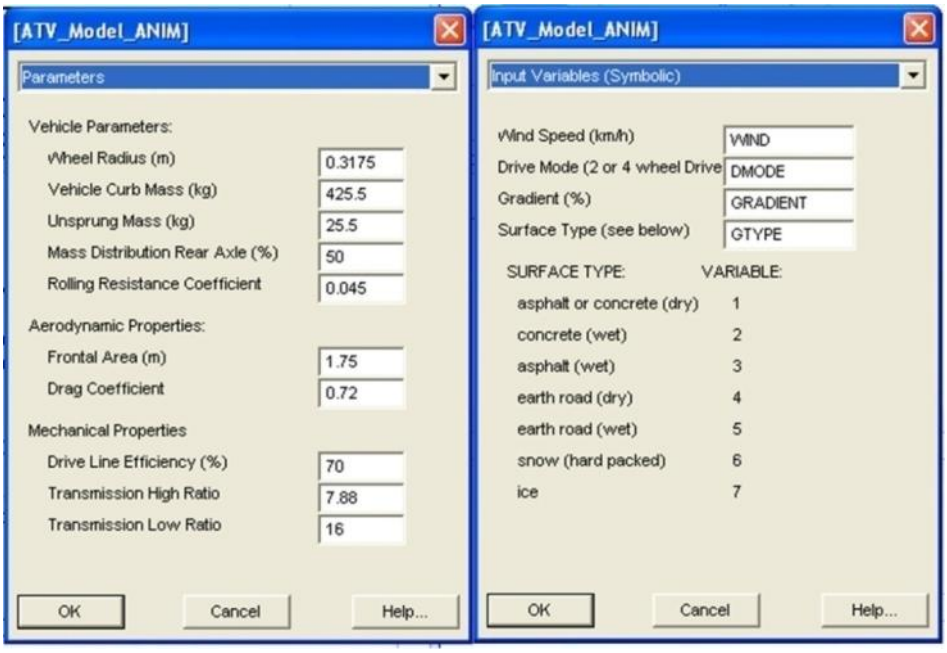

Figure 3.7 - PSCAD ATV model parameter input dialogs

The model also includes the ability to monitor all of the forces, both internal and external to the vehicle. These forces are output through user assigned variables that can be entered through the output variables dialog of the model shown in Figure 3.8. The outputs also include wheel slip and wheel rpm to allow the user to see the effect of the different ground types on the vehicle.

Figure 3.8 - PSCAD ATV model output variables dialog

A manufacturer-provided acceleration curve was used to validate the performance of the mechanical model. The curve provided by the manufacturer was documented using an ATV that was powered by an ICE through the CVT. In order to have a true comparison, a torque curve was generated that closely resembled that of the ICE-CVT combination. This curve was used to compare the model to a real test. The test curve is shown in Figure 3.9, there are slight variances in the acceleration primarily due to the curve fitting. The maximum speeds achieved during the test are practically identical after 40 seconds.

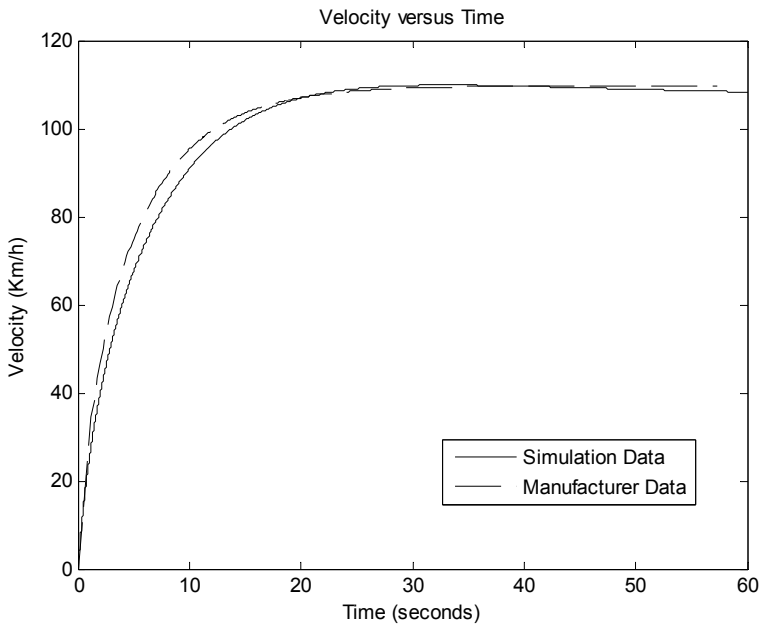

Figure 3.9 - Graph of model data versus Polaris data

3.4.2 Electrical Machine Model

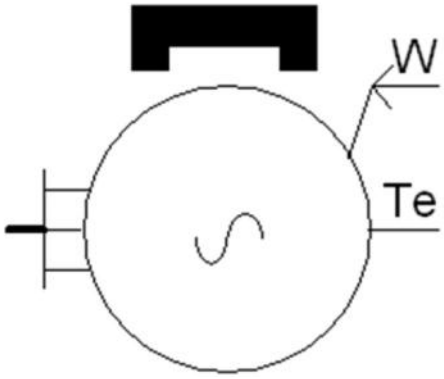

Figure 3.10 - PSCAD master library PM machine model

To model the permanent magnet synchronous machine (PMSM) selected in section 3.3.1, the PMSM component from the PSCAD master library is used. The PMSM component, shown in Figure 3.10, connects directly to a three phase electrical network or

controller through the wire connection seen the left side. The right side is the electrical speed input and the electrical torque output of the machine. Both of these values are in pu and must be scaled appropriately to connect to the mechanical load model. The inductance and resistance parameters of the machine also have to be input to the model in pu. Table 3.5 includes the rated values of the machine from the manufacturer's datasheet as well as the appropriate values converted to per-unit (pu).

Table 3.5 - Perm PMS-150 Motor Parameters

Parameter	Rated Value	PU value (pu)
Rated Power	13.0 kW	1.0
Voltage	66.5 $V_{ll\text{-}rms}$	1.0
Current	151 A_{rms}	1.34
Speed	4500 rpm	
Torque	27.5 Nm	1.0
Torque Constant (k_T)	0.182 Nm/A	-
Voltage Constant (k_e)	11.17 V / 1000 rpm	-
Poles	8	-
Frequency	300 Hz	1.0
Winding Resistance	6.46 mOhm (ph-ph)	0.0095
Inductance	0.0385 mH (ph-ph)	-
D, Q-axis Reactance @ 300 Hz	-	0.1588

The machine closely resembles a non-salient synchronous machine in that is has three phase windings on the stator and the rotor has a dc field. In the case of the PMSM, the rotor field flux is supplied from the permanent magnets rather than an external supply, allowing the machine to be more efficient. The flux linkages of the equivalent dc field of the magnets induce a sinusoidal back emf in the stator windings, with the peak dependant on the location of the rotor. To simplify the analysis of the machine, the d-q transformation from [18] is used to transform the machine variables, using the rotor position, into an orthogonal reference frame that rotates synchronously with the rotor.

This transformation removes the position dependence of the flux linkages allowing the circuits to be analysed using dc voltages.

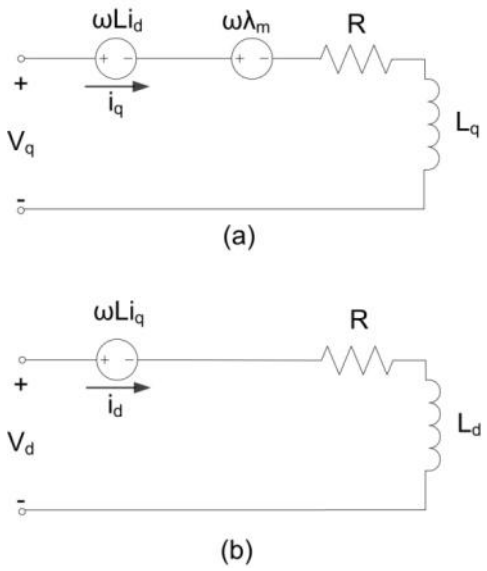

Figure 3.11 - (a) The q-axis and (b) the d-axis equivalent circuits of the machine

$$V_q = ri_q + \omega L i_d + \omega\lambda_m + L\left(\frac{di_q}{dt}\right) \tag{3.13}$$

$$V_d = ri_d - \omega L i_q + L\left(\frac{di_d}{dt}\right) \tag{3.14}$$

Equations 3.13 and 3.14 are the results of the transformation and can also be represented as the equivalent circuits shown in Figure 3.11. In these equations, V_q and V_d are direct (d) and quadrature (q) axis voltages, i_q and i_d are the d and q axis currents, r the phase resistance, L the phase inductance, λ_m represents the back emf constant and ω (electrical rads/sec) is the rotor angular velocity. The first term in both equations

represents the stator resistance voltage drops. The second terms are known as the speed voltage terms as they represent the change as a function of speed and current the cross-coupling of the fields. The third term of 3.12 represents the back emf due to the permanent magnet. The final term of both equations accounts for the voltage drop across the inductance. This term is only prevalent during transients and can be neglected in the steady state. Equation 3.15 is an approximation of the electrical torque of a nonsalient pole PMSM, where k_T is the motor torque constant. This constant is a function of the motor parameters and the magnetic field intensity of the permanent magnets, which is essentially constant for a PMSM.

$$T_e = k_T i_q \tag{3.15}$$

3.4.3 Control System Development

One of the design requirements of the project is to have the ATV operated in the same fashion as conventional ATVs. These ATVs are driven by a thumb actuated throttle lever which is identical in function to the gas pedal found in on-road vehicles. When the pedal is actuated the user is requesting the ICE to generate a force to accelerate the vehicle. A request for more force than the load forces will accelerate the vehicle. In the same way, a request of less force than the changing load forces will decelerate the vehicle.

Take for example a vehicle approaching a hill. If the driver of the vehicle maintains the same pressure on the gas pedal from before the climb, the vehicle will begin to slow due to the increase of load force the hill has added to the vehicle. If the gas pedal was tied to a vehicle speed instead of a force, the vehicle would have commanded more

torque from the ICE to maintain the same speed under the changing load condition. From this example it can be seen that tying the throttle lever to a torque reference to control the torque of the motor will afford the user the same feel as would operating a conventional ATV.

From equation 3.15 the torque of a PMSM can be controlled directly by controlling the q-axis current. The maximum torque per ampere, and thus the maximum efficiency of the machine, can be obtained by setting i_d to zero and controlling the magnitude of i_q. A positive current will result in a positive electrical torque developed by the motor and a negative (or braking torque) can be developed by a negative current. Controlling the d-axis current of the machine is equivalent to controlling the field current in a separately excited dc machine. The injection of a negative d-axis current would effectively reduce the field strength of the permanent magnets and allow for limited operation in the field weakening, or constant power region, (see [19], [20] if further details about constant power operation of a PMSM are required).

The torque control block diagram is shown in Figure 3.12. The torque request T_{in} is converted to a current command by a feed forward current synthesizer based on the motor's torque constant. The output of the current synthesizer is a rate limiter to smooth the overall response and limit the rate of change of current. This current command is passed through a feedback current regulator in the form of a PI controller. As the motor equations are cross-coupled, the speed voltage terms are added after the current regulators to decouple the control. This decoupling improves the current regulator response, achieving improved and accurate tracking of the commanded currents [20]. The back emf of the machine, $\omega\lambda_{m,}$ is a linear function of speed and can therefore be

added to the q-axis control to speed-up the control loop, and reduce the burden on the q-axis current regulator.

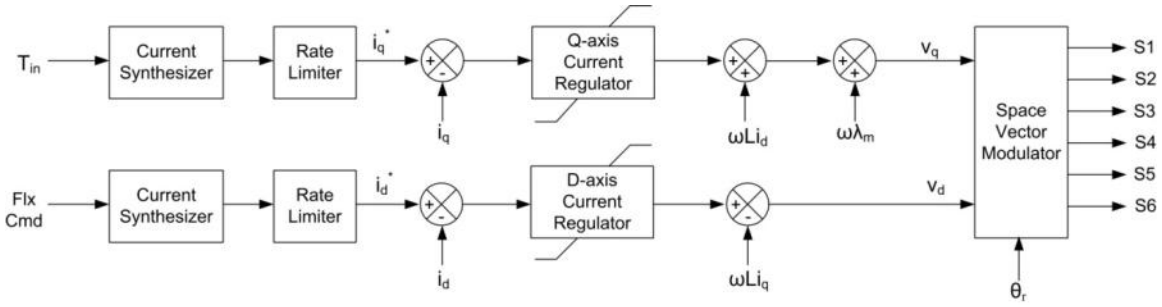

Figure 3.12 - Block diagram of decoupled torque control

3.4.3.1 Firing Pulse Generation by Centre aligned Space Vector Modulation

Having determined the required d-axis and q-axis voltages to generate the commanded torque, gate signals must be calculated in order to generate the proper phase voltages to apply to the motor terminals. Centre aligned space vector modulation (SVM) is used as the modulation scheme as the gate signals can be calculated directly from the rotor reference frame voltages and the rotor position data. An added benefit to centre aligned SVM is the effective doubling of the switching frequency and overall reduced total harmonic distortion (THD) [21].

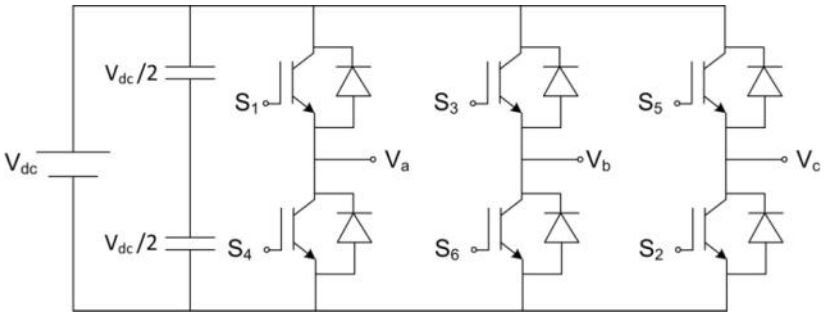

Figure 3.13 - Schematic of a two-level voltage source converter

SVM uses the different switching states of the converter (shown in Figure 3.13) to produce a state vector. The two switches in each leg of the converter cannot be in the same state at the same time. If both switches are on, the leg will short circuit the dc bus. If both switches are off there will be an open circuit. The switches are therefore operated in complementary states. When the upper switch is on, the mid-point is connected to the positive dc bus. When the lower switch is on, the mid-point is connected to the negative dc bus. As the converter has three legs, there are a total of 8 potential converter states corresponding to 6 space vectors each 60 degrees apart (forming 6 evenly spaced sectors) and two zero-value vectors. The eight states and their corresponding phase voltages are described Table 3.6 and are also shown in Figure 3.14, where the states are numbered in binary, corresponding to the upper switch (1 for on, 0 for off). The left most zero is the switch in leg C, followed by leg B and finally leg A.

Table 3.6 - Space vectors and corresponding phase voltages

State	S1	S3	S5	Phase Voltage		
				V_{an}	V_{bn}	V_{cn}
0	0	0	0	0	0	0
1	0	0	1	$\frac{2V_{dc}}{3}$	$-\frac{V_{dc}}{3}$	$-\frac{V_{dc}}{3}$
2	0	1	1	$\frac{V_{dc}}{3}$	$\frac{V_{dc}}{3}$	$-\frac{2V_{dc}}{3}$
3	0	1	0	$-\frac{V_{dc}}{3}$	$\frac{2V_{dc}}{3}$	$-\frac{V_{dc}}{3}$
4	1	1	0	$-\frac{2V_{dc}}{3}$	$\frac{V_{dc}}{3}$	$\frac{V_{dc}}{3}$
5	1	0	0	$-\frac{V_{dc}}{3}$	$-\frac{V_{dc}}{3}$	$\frac{2V_{dc}}{3}$
6	1	0	1	$\frac{V_{dc}}{3}$	$-\frac{2V_{dc}}{3}$	$\frac{V_{dc}}{3}$
7	1	1	1	0	0	0

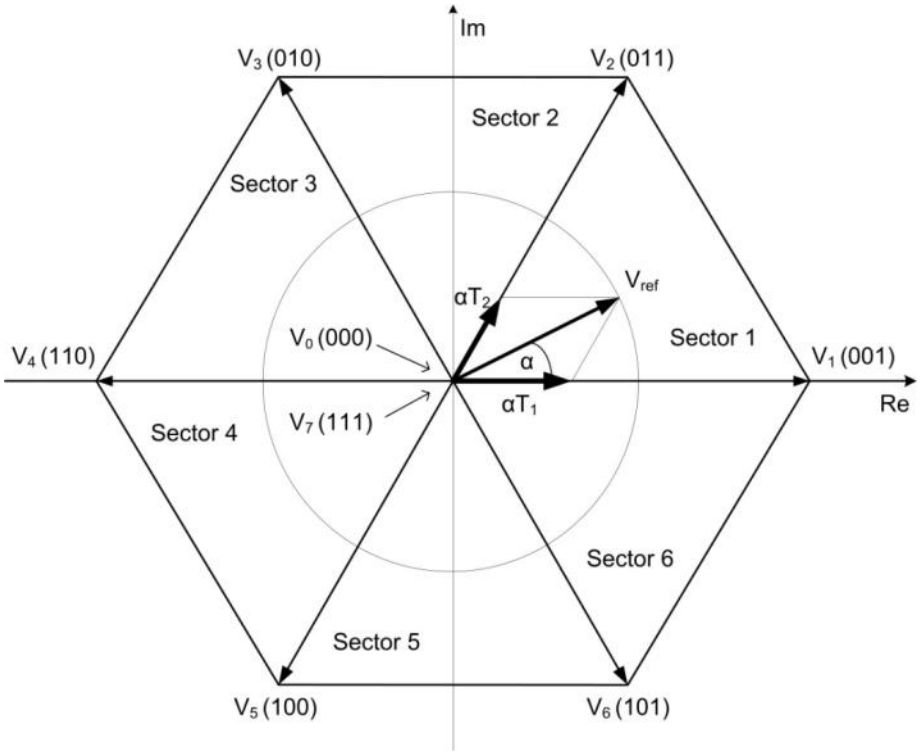

Figure 3.14 - Space vector diagram for two-level SVM

By using equation 3.16 any balanced set of three phase voltages can be represented in the same two-dimensional plane as shown by the reference vector V_{ref}.

$$V_{ref} = \frac{2}{3}\left(v_a(t) + v_b(t)e^{j\frac{2\pi}{3}} + v_c(t)e^{-j\frac{2\pi}{3}}\right) \tag{3.16}$$

The reference vector can then be mapped to the two vectors that border the sector the reference is located in (i.e. the vector is located in Sector 1 in Figure 3.14) and either of or both of the zero vectors according to equation 3.17., the vectors V_0 and V_7 represent the zero vectors and V_l and V_u respectively represent the lower and upper valued vector

of the current sector and the times T_0, T_1 and T_2 are further defined by equation 3.18, 3.19 and 3.20 respectively.

$$V_{ref} = \frac{T_0 \cdot V_0 + T_1 \cdot V_l + T_2 \cdot V_u + T_7 \cdot V_7}{T_s} \tag{3.17}$$

$$T_1 = \frac{\sqrt{3}}{2} \cdot T_{pwm} m \cdot sin\left(\frac{\pi}{3} - \theta\right) \tag{3.18}$$

$$T_2 = \frac{\sqrt{3}}{2} \cdot T_{pwm} m \cdot sin(\theta) \tag{3.19}$$

$$T_0 + T_7 = T_{pwm} - T_1 - T_2 \tag{3.20}$$

The m in equations 3.18 and 3.19 represents the modulation index of the vector defined by equation 3.21 and T_{pwm} is equal to the sampling period and is equal to the inverse of the sampling frequency.

$$m = \frac{V_{ref}}{V_{dc}/2} \tag{3.21}$$

In centre aligned PWM, the zero vector time is split between both zero vectors. The switches are fired in a forward sequence followed by a reverse sequence. This is also referred to as a back-to-back firing scheme. The times can be recalculated and updated at the beginning of a new period, or every T_{pwm}. This takes advantage of both zero vector states to minimize the number of switchings effectively doubling the sampling frequency

as shown by the timing diagram Figure 3.15. The timing diagram illustrates the effective doubling of the sampling frequency by showing two periods placed back-to-back. The duty cycle of the switches is adjusted after one period even though the switches have the appearance of going through only one period of twice the length. In this diagram the actual switching period is $2 \bullet T_{pwm}$, while the effective switching period is T_{pwm}.

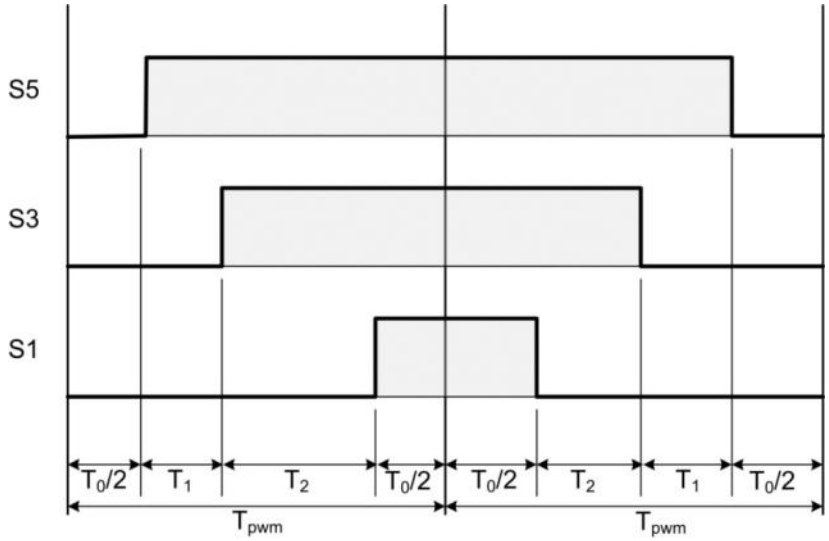

Figure 3.15 - Timing diagram of centre aligned space vector modulation.

A custom component that generates the necessary firing pulses, according to centre aligned SVM, is shown in Figure 3.16 and is written for use in PSCAD. It is located with the DSP page module of the simulation case. The block also incorporates the interpolation features as described in [22], to decrease the overall simulation time.

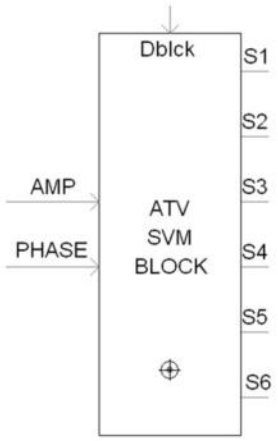

Figure 3.16 - Custom SVM firing pulse block

3.4.4 Battery Model

There are multiple battery models that exist that try to mathematically reproduce the chemistry effects of batteries. These models include lumped resistor and capacitor networks, and detailed physics based models. These models can be complex and require plenty of additional calculation overhead for little impact on the mechanical system simulation results. For further information about Li-ion battery modeling please refer to [23].

For the purposes of the simulation, the battery has been represented as an ideal voltage source with an equivalent series resistance. This simplified model has been assembled in such a way that it easily allows for the addition of a more sophisticated battery model in the future.

3.4.5 Overall Model Overview

The complete model including the mechanical ATV load, PMSM motor, control system, batteries and power electronic switches as laid out in PSCAD is shown in Figure 3.17. To make the case easier to navigate, portions of the case have been included in

page modules. These include the control system, the VSC, the battery, and the load model. Also included in a page module is a representation of the digital controller. This has been done with the purpose of replicating the actual controller functionality. Typical controllers have limited mathematical capabilities as well as a limited range for data. These limitations have been built into the case and will be discussed in the next chapter.

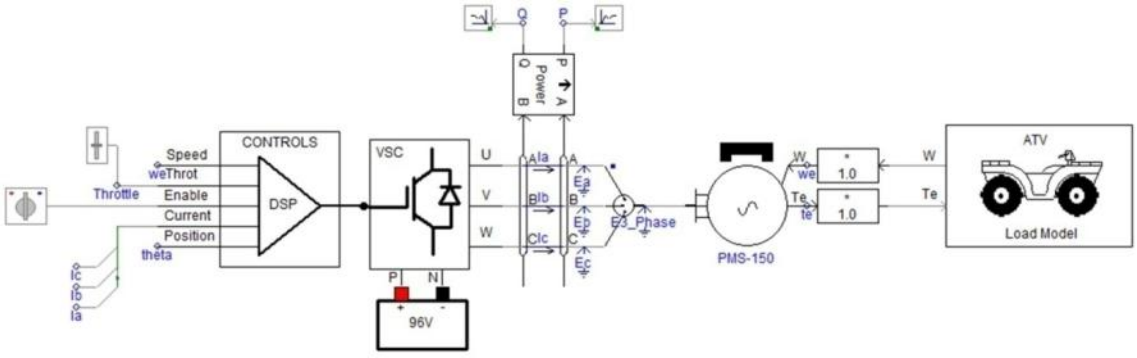

Figure 3.17 - PSCAD ATV simulation case

3.5 Tuning of the Current Regulators using Simplex Optimization

The two PI based current regulators of the motor controllers must be setup correctly in order to function. Ideally, the current regulators will be tuned such that the measured current is equal to the requested current. This can easily be achieved in the steady state even with poorly tuned controllers. To achieve the requested steady state currents quickly and to respond to disturbances in the system, the controllers must be tuned well. Each of the two current regulators has two parameters that require tuning. The first parameter, K_p, is the proportional gain constant and the second parameter, K_t, is the integral time constant. A benefit of simulation modeling in PSCAD is the ability to use

the simplex optimum run component to tune the parameters. This component is based on the simplex optimization routine described in [24].

The overall goal of the current regulators is to deliver the requested current with the least amount of current ripple. In order to use the built in optimization feature of PSCAD, the parameters are first selected manually and the simulation results observed. Once the system responds as expected, an objective function is created. The objective function is required as an input to the simplex optimum run block. In this case the objective function, described by equation 3.22, is the error between the current reference and the measured current. This error is then squared to penalize equally a positive error and a negative error. An integrator is used to accumulate this error over the length of the run. Both accumulated errors are then added together. The simplex optimization setup as described is shown in Figure 3.18.

$$O.F. = \int \left\{ \left(I_q^* - I_q\right)^2 + (I_d^* - I_d)^2 \right\} \tag{3.22}$$

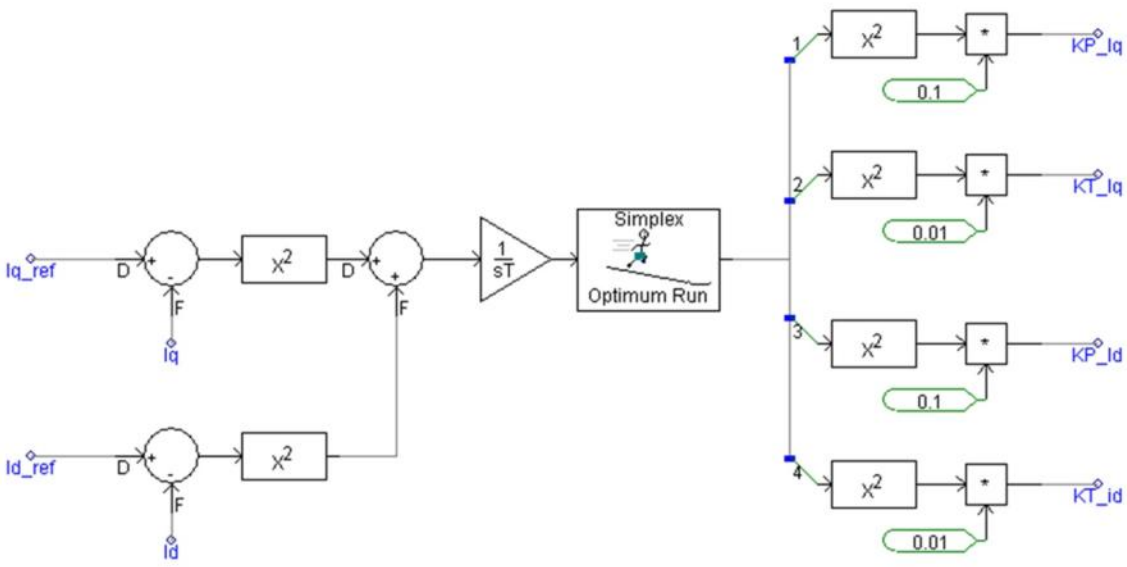

Figure 3.18 - Simplex optimization system for current regulators

The output of the optimum run block is four variables which are squared, to eliminate negative values, and scaled appropriately. These variables are assigned to their designated current regulator parameter for the next run. The block will re-run the simulation trying new values until either the tolerance is met or the number of runs exceeds the limit. The block is configured as shown in Table 3.7

Table 3.7 - Simplex optimum run block settings

Parameter	Value
Optimization method	Simplex
Number of real variables to control	4
Maximum number of multiple runs	1000
Tolerance	0.0005
Initial step size	0.1

To reduce the amount of time required to perform the optimization, a simple throttle input is used which consists of the driver first linearly increases the throttle over five

seconds and holding it at full throttle for a five second interval, followed by a linear drop to zero over a further five second interval. The results of the simplex optimization are shown in

Table 3.8 and will be used as starting values for tuning the current regulators of the prototype ATV.

Table 3.8 - Results of optimization

Parameter	Initial Value	Optimum Value
Q-axis K_p	0.09	0.04
Q-axis K_t	0.049	0.003
D-axis K_p	0.09	0.74
D-axis K_t	0.049	0.138
Objective function	15.2	10.4
Number of runs		177

3.6 Evaluation of the Simulated Vehicle Performance

To evaluate the performance of on-road vehicles, known drive cycles are used to compare the vehicle with existing data. As an ATV is subjected to vastly different uses and terrains than typical on-road vehicles, there are no existing drive cycles that can be used. To obtain a reasonable picture of performance of the ATV straightforward test are undertaken. These tests are additional to test already performed to confirm the suitability of the mechanical load model. The tests include (i) acceleration tests on different terrain types, (ii) a coast down test and (iii) a terrain change test.

Using the complete simulation case, acceleration tests are performed using different ground types to determine the effects on the top speed and acceleration time of the vehicle. In addition to this, the difference in wheel slip and motor power are also recorded. The acceleration test is performed by applying maximum motor torque until the top speed of the electrical motor is achieved. A summary of the results of these test

are found in Table 3.9. The maximum speed achieved by the electric ATV is 67.8 km/hr after 15.5 seconds. A graph of this test can be seen in Figure 3.19. This is a direct result of the electrical motor reaching its rated speed of 4500 rpm. The motor has not yet reached its rated power leaving room for overcoming added ground resistance or a head wind without losing top speed. Wet asphalt and gravel have a slight effect on the top speed as the wheel slip has increased.

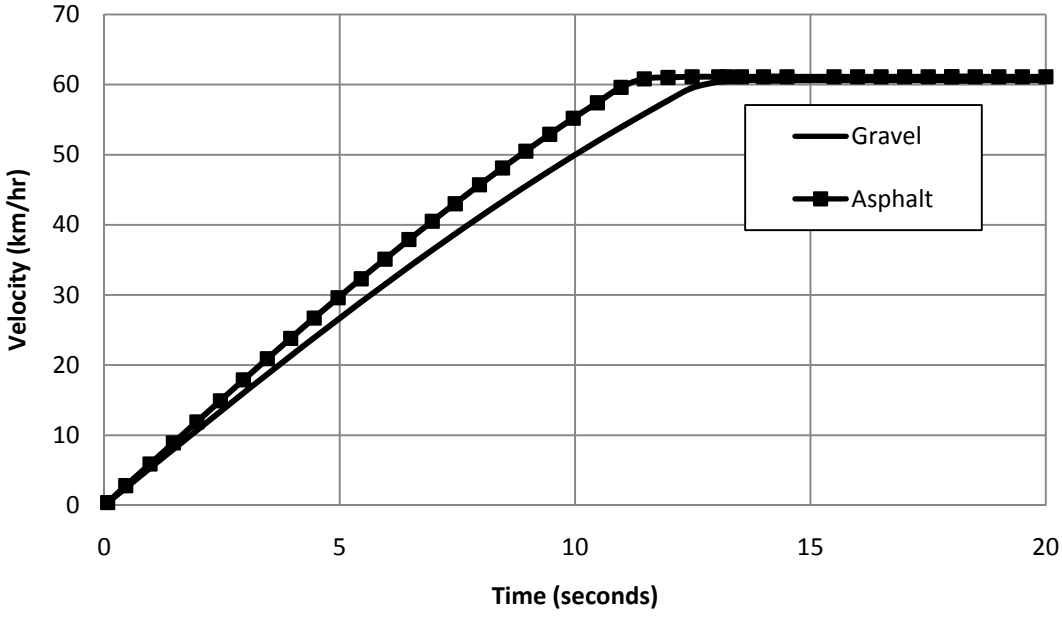

Figure 3.19 - ATV acceleration test on asphalt and gravel

While running in snow the ATV's top speed is significantly less, primarily because the motor is at rated power to overcome the added rolling resistance of the snow. Two-tests were performed in snow. The first is in rear-wheel drive and the second in AWD. The key difference is the reduction in wheel slip in AWD. There is no effect on the top speed seeing that in both cases the motor reaches rated power. There is however, a

noticeable decrease in the time it takes to accelerate to the top speed. This is principally for the reason that in AWD more tractive effort effectively reaches the ground.

When tested on ice as a ground type, the ATV is capable of applying only 55% of rated torque, which results in a wheel slip of 13.5%. If the torque is increased any further it will result in the wheels spinning in place and the electric motor reaching rated speed rapidly. The decrease in top speed is a direct result of the limit on the torque that can be applied.

Table 3.9 - Acceleration test results for different terrain types

Terrain Type	Top Speed (Km/hr)	Acceleration Time (s)	Wheel Slip (%)	Power (kW)
Asphalt (dry)	67.8	15.5	1.08	9.55
Asphalt (wet)	67.0	16.2	1.91	9.40
Gravel	66.9	18.1	1.96	11.56
Snow (RWD)	48.4	22.1	7.61	13.19
Snow (AWD)	48.9	20.5	2.15	13.23
Ice (AWD) 55% rated Torque	30.12	15.0	13.5	4.95

A coast down test is carried out by first accelerating the ATV to its top speed, at which point the motor torque is set to zero. The resulting decrease in speed is a consequence of the aerodynamic drag at high velocities. Figure 3.20 is a speed versus time plot of a coast down test of the ATV on asphalt and gravel. The coast down time from the same top speed until stop is 37 seconds on asphalt and 27 seconds on gravel. This demonstrates the effects of a larger rolling resistance on the coast down of a vehicle.

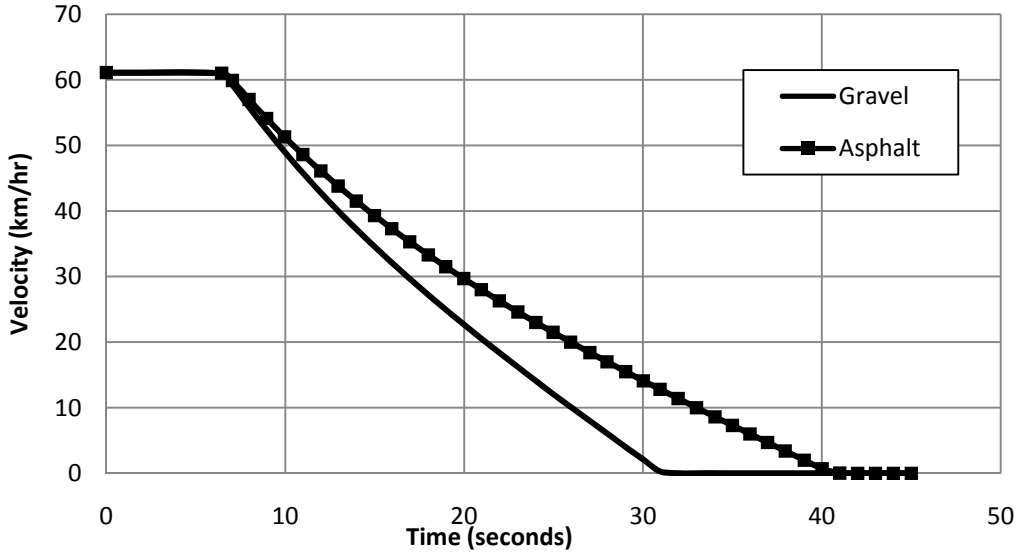

Figure 3.20 - Coastdown test of ATV on asphalt and gravel

A terrain change test is completed by applying a constant torque to reach a desired speed and the changing the terrain that the ATV is driving on without changing the torque set point. Figure 3.21 is a speed versus time plot of a step change in the ground type. In this test, torque is applied to maintain a speed of 57.0 km/hr, the terrain is then changed from asphalt to earth road, the increase in rolling resistance as a result of the soft dirt decreases the top speed by a substantial 17%. This test could be performed for any change in terrain type for which the effects on the vehicles rolling resistance and maximum tractive effort are known.

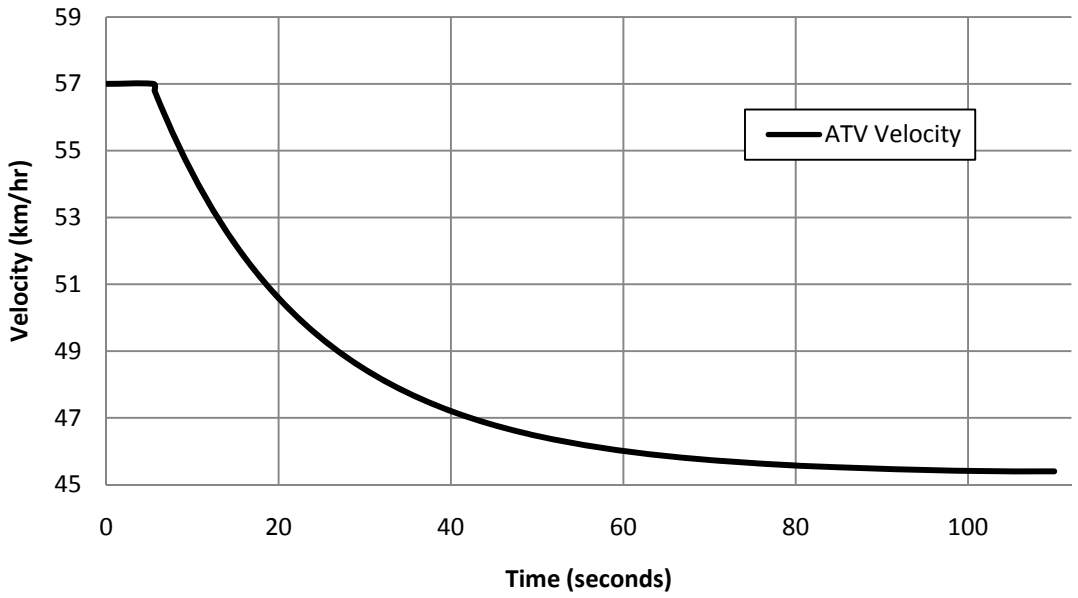

Figure 3.21 - Effects of a step change in terrain type (from asphalt to earth road)

Having tested and optimized the control approach for the electric ATV, as well as performed some uncomplicated tests of the vehicle's overall performance, implementation of the vehicle can be done to confirm the simulation results.

4 IMPLEMENTATION

4.1 Overview

In order to confirm the simulation results obtained using PSCAD, a prototype of the electrical vehicle is constructed. This chapter will describe how the primary components are selected from the simulation studies. As outlined in Chapter 1, the commercial ATV will have to be modified to house the electrical drive train within its frame and the entire electrical system will have to be built from the ground up to work with the new components. A description of the selected vehicle control unit and the coding approach used are also detailed. Lastly, secondary systems are also discussed that have been implemented in the prototype for energy efficiency and to assist the user with feedback from the drive systems.

4.2 Primary Component Selection

Preliminary selection of the electric motor and batteries is discussed in Chapter 3 for use in the simulation stage. Following the simulation, it is determined that the electrical motor and battery voltage level selected have the ability to meet most of the requirements of the vehicle. After confirming that there is enough space on the vehicle to indeed fit both the PERM PMS-150 electric motor and five 19.2V battery packs required to achieve 96V, the specified components will be used in the prototype. The following details these and other important components to be used on the electric ATV.

4.2.1 PERM PMS-150 Permanent Magnet Synchronous Motor

The selected electric machine, the PERM PMS-150 as detailed in Chapter 3 and shown in Figure 4.1, has been selected. The motor is a 13kW axial flux permanent magnet synchronous machine with dual three-phase stators, making it very compact and energy efficient. It is the compactness of the machine that allows it to be installed into the ATV frame with relative ease. A benefit of the machine is that it has the capabilitie to produce 300% of rated torque for periods of up to 10 seconds, allowing it to generate up to 80Nm of torque if required. This torque exceeds the peak torque output of 50Nm that the original ICE generates. The motor has a built in analog resolver that is used for the position feedback of the rotor. A temperature sensor is also integrated into the machine to monitor the temperature and to ensure that rotor permanent magnets stay within the specified limits.

Figure 4.1 - PERM 96V 13.0 kW PMSM

4.2.2 Valence UEV-18XP U-Charge XP series Li-Ion Batteries

The battery selection is one of the most challenging decisions due to the vast selection of different technologies that are currently available and still under development. To limit added weight to the vehicle, Li-ion batteries were selected because they have the highest energy density available and are relatively compact for their power and voltage ratings.

Li-ion batteries are very challenging to use as they have very specific charge requirements and are particular in their discharge depth and cycle. Valence Technology offers a complete battery system. Each of the batteries contains the required electronics to monitor the state of each internal cell and can communicate this data to the battery management module. Four of the five 19.2V battery packs are shown in Figure 4.2.

Figure 4.2 - Valence UEV-18XP lithium-ion battery packs

The battery management module shown pre-wired in Figure 4.3 has the ability to control the main dc relay of the vehicle, as well as, the pre-charge and charger relays that will be discussed later. This greatly reduced the amount of time necessary to safely enable and disable the electrical systems. In the event of a battery emergency or an over-discharge of the batteries beyond their limit, the battery management has ultimate control over the main and charger relays and can disconnect them if needed. The module also monitors the current state-of-charge of the batteries and has a linear analog output that can be used to gauge the remaining charge.

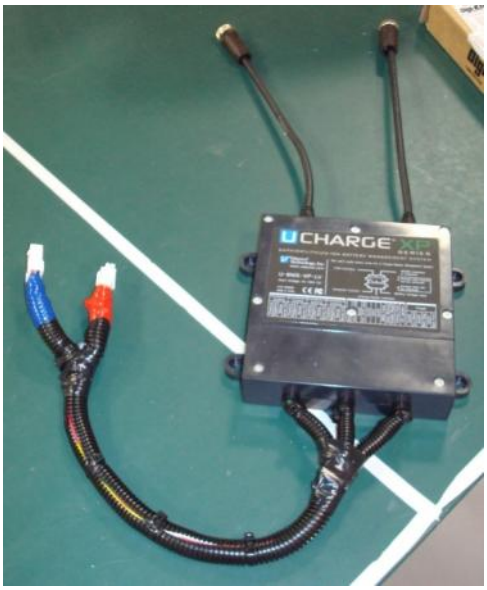

Figure 4.3 - Valence U-ChargeXP battery management module

4.2.3 Delta-Q 96VQuiQ Battery Charger

As Li-ion batteries are very specific regarding their charging characteristics, A 96V QuiQ charger from Delta-Q has been selected for use on the ATV, shown in Figure 4.4. Delta-Q has programmed the charger, as requested by Valence Technologies, for the

specific set of batteries that is used on the ATV. Added benefits to the QuiQ charger are the abilities to withstand harsh environments and to mount directly to the ATV frame. This will allow for easy charging from any 120V outlet, not limited to locations where a permanent charging station is installed. The charger delivers 1kW of power to charge the battery, permitting a complete recharge of the selected batteries in 4 to 6 hours from any standard 120V outlet. The charger also has an interlock feature that can be used to lockout the vehicle's ability to drive when the charger is plugged into an outlet.

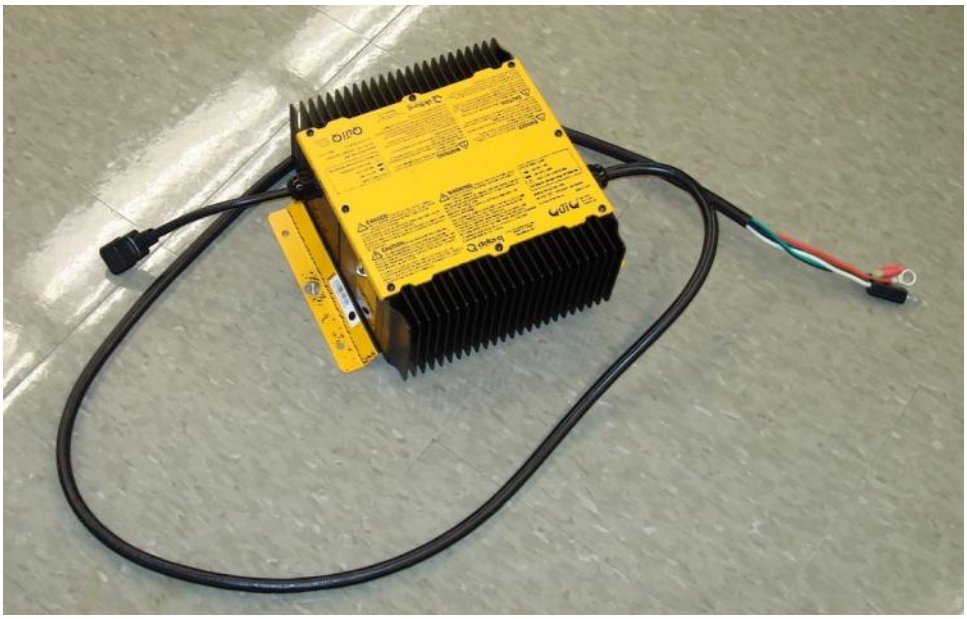

Figure 4.4 - Delta-Q 96 V , 12 A battery charger

4.2.4 96 V to 12 V Isolated dc/dc Converter

The control and auxiliary systems such as the lighting, speedometer pod, motor controller require 12V. To reduce the risk of electric shock and exposure to the 96V system, a 96V to 12V dc/dc converter is used, shown in Figure 4.5. This converter

isolated the ground of the 96V system from that of the 12V system, allowing the frame to be used as the 12V systems ground. This allows for easy connection grounding of the lighting, and control system's without exposing the driver to the 96V system. The selected dc/dc converter has a power rating of 350W and an efficiency rating of 83%. The dc/dc converter also has built in protection for over-currents and over-voltages.

Figure 4.5 - 350W, 96V to 12V dc/dc Converter

4.2.5 Motor Drive Components

The motor drive has multiple components that require selection. Based on the motor ratings an IGBT module was selected. IGBTs were selected as the switch of choice for their low loss at the required current levels, as well as their ability to switch at

frequencies of up to 20 kHz. The selected insulated gate bipolar transistor (IGBT) module is an intelligent power module from Powerex containing the six IGBTs required for three-phase control of the motor. The module incorporates integrated protection for short circuits, over temperature and under-voltage, reducing the time required for protecting circuit design. The module also facilitates the implementation of the gate drive circuits by using a gate drive board available from the manufacturer. A snubber capacitor capable of limiting the voltage rise across the device, selected according to the IGBT manufacturer recommendations, is installed across the dc bus terminals. 400 uF of filter capacitance is also installed using low equivalent series-resistance (ESR) film capacitors provided by electronic concepts. All of the motor drive components are assembled in a weather-proof enclosure with water-tight connectors on all cables and control wiring entering the box. Figure 4.6 shows the complete assembly including: (A) the dc filter capacitors, (B) the snubber capacitor (below the copper dc bus), (C) the gate drive board, (D) motor phase terminals, (E) the dc bus.

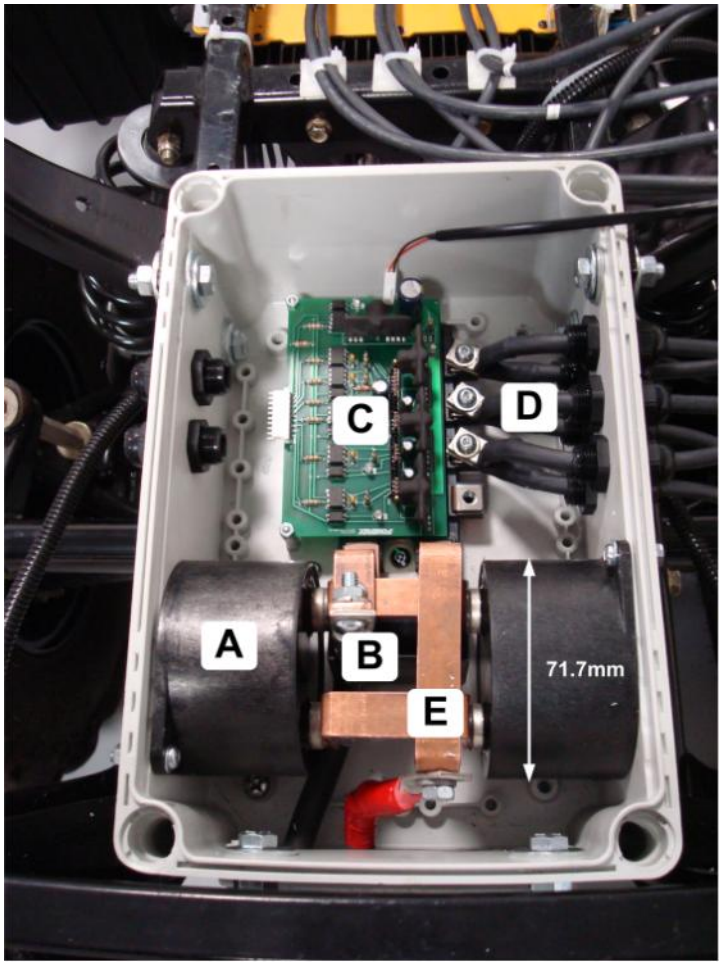

Figure 4.6 - Motor drive enclosure

4.3 ATV Modification

Before the installation of the new components could begin, the frame of the ATV had to be modified to accommodate the placement of the motor and batteries. The ATV was first stripped down until only basic components remained on the frame, shown in Figure 4.7. Space was opened up on the frame by removing the ICE supports and mounts. A plate to support the motor was installed and mounts for all five of the batteries were built into the frame. The battery mounts allow for rubber damping to be installed between the

batteries and the frame, which isolates vibration. The mounting also allows for easy interconnection of the battery cables and battery management communication cables.

Figure 4.7 - ATV frame before modification

The ATV frame after the modifications are complete is shown in Figure 4.8. The motor is mounted to the newly installed support plate (A) and the lower 4 battery mounts (B, C, D, E) one upper battery mount (F) are labelled. The batteries in the lower mounts will be installed upright and the upper mount will have a battery installed on its side. Having the vehicle completely apart also allowed for painting and cleaning of the frame and all components. Any components that were originally red have been painted black to give the vehicle a clean and simple appearance.

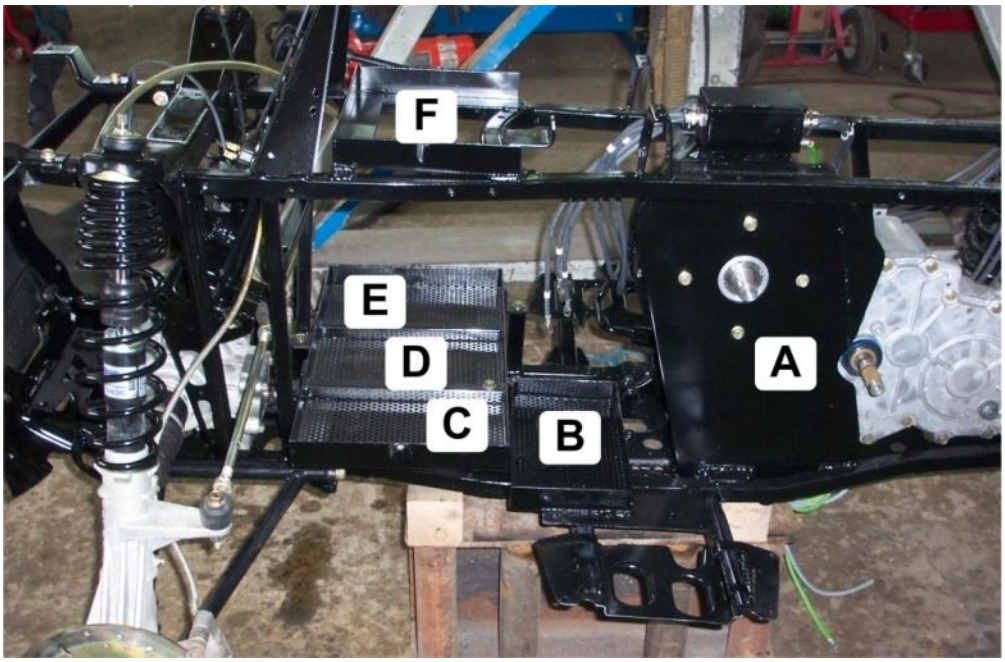

Figure 4.8 - ATV frame after modifications

The completed frame modifications with the motor and batteries installed, including the rubber damping is shown in Figure 4.9. In the image, the original gearcase is visible as well as the original suspension and drive axle components.

Figure 4.9 - Completed ATV mechanical modifications

Figure 4.10 shows the cogged belt selected as a mechanical coupling to connect the shaft of the electrical motor to the input shaft of the gearcase. Also shown in this figure is the mounting location of the battery charger. This method was selected, along with a fixed tensioning pulley in order to facilitate power transfer from the motor to the gearcase, as well as from the wheels to the motor in the case of regenerative braking. The ratio for the mechanical coupling was selected using results from the simulation in order to achieve a reasonable top speed without reducing the motor torque substantially. The ratio selected is an increasing ratio of 1 to 1.35. This allows for peak rpm input to the gearcase of 6075 rpm, which is near the input speed from the original CVT.

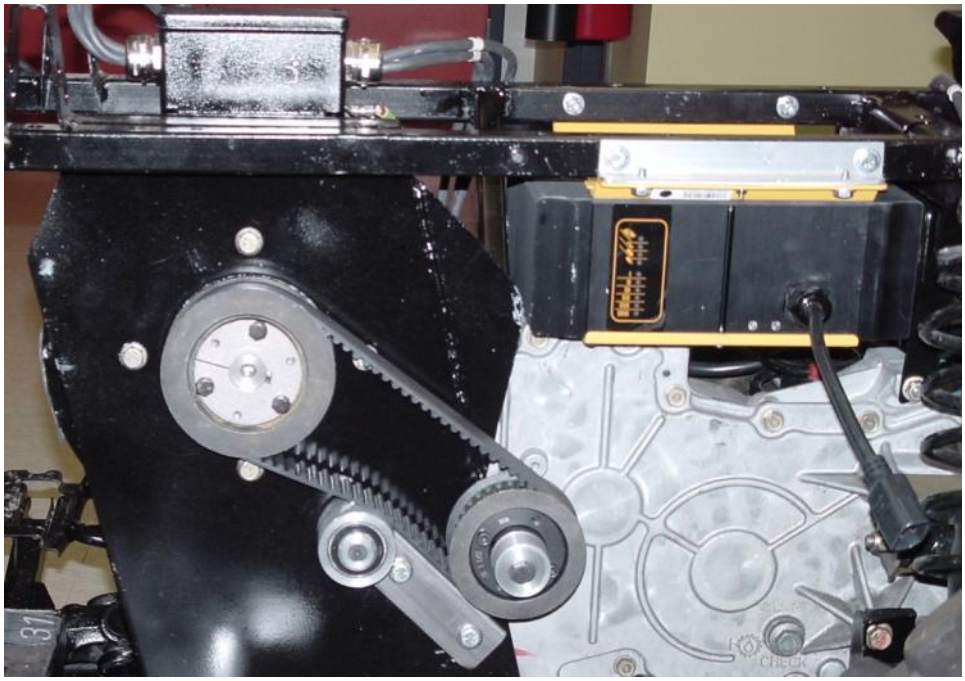

Figure 4.10 - Mechanical coupling between the motor and gearcase

The completed mechanical alterations to the vehicle allow for the installation of the remaining electrical and control components to be installed.

4.4 Electrical System

The electrical system consists of a 96V and a 12V system that are isolated by the dc/dc converter. As mentioned above, the 12V system is grounded to the vehicle frame, referred to as the chassis ground, and the control signals originating in the 12V system that are required to drive the IGBT switches are isolated through opto-isolators. These opto-isolators prevent possible high voltage transients from damaging the low voltage equipment. Figure 4.11 is a basic electrical system overview. The diagram shows the 96V system connections and control relays. These relays, C1, C3 and C4, are controlled by the battery management system (BMS). When the vehicle key-switch is enabled, the

battery management first closes the pre-charge relay (C3) for 2 seconds. C3 connects the dc-filter capacitors to the battery through a 100 ohm resistor to limit the in-rush current due to the capacitors. The main relay (C3) is then closed and the pre-charge relay is opened. This sequence also enables the dc/dc converter activating the 12V system for the control and auxiliary equipment.

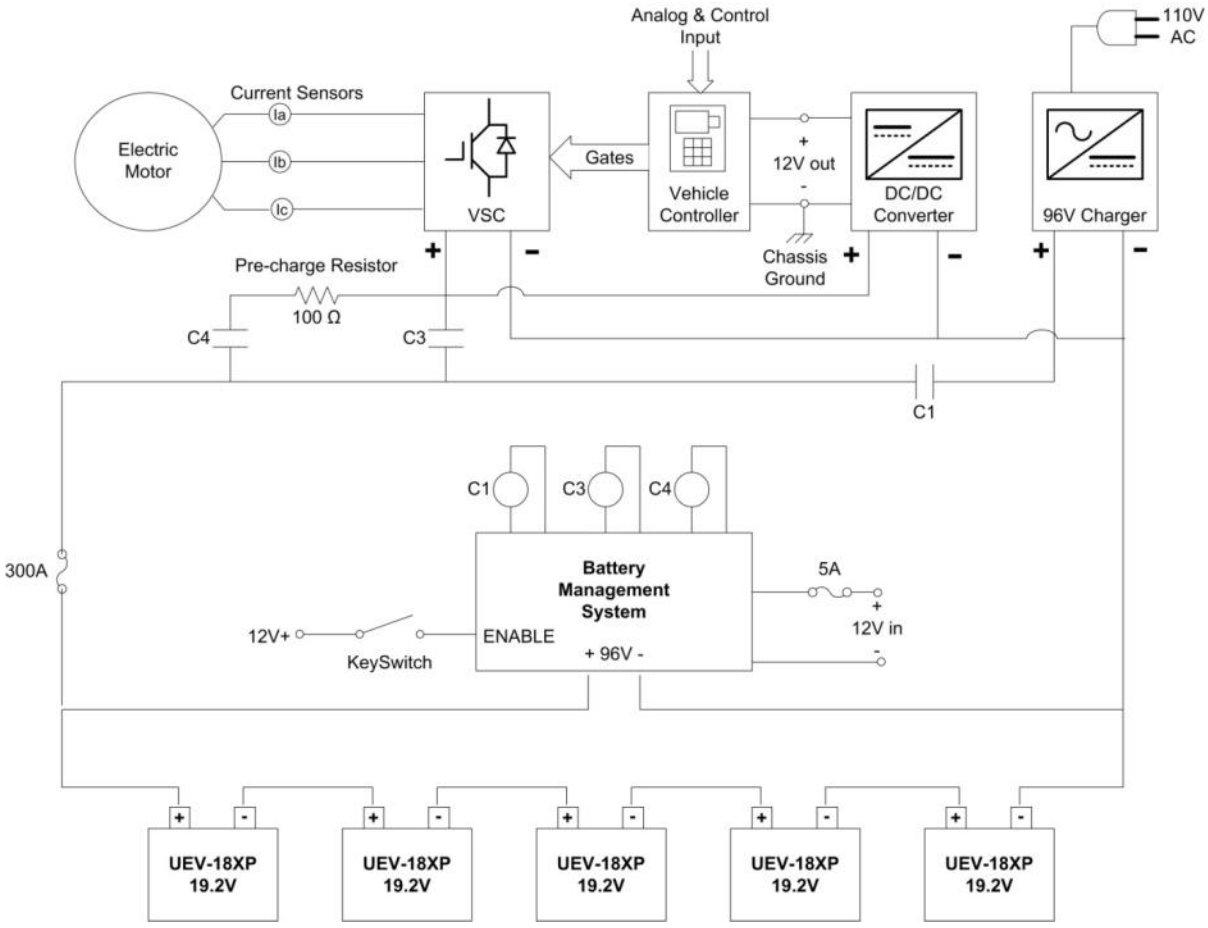

Figure 4.11 - Basic electrical system overview

To charge the batteries the charger is first plugged into a 120V outlet. The BMS then disconnects C3 and C4, if necessary, locking out the motor drive before connecting C1 to allow the charger to control the charge to the batteries.

If at any time the BMS detects a problem with any of the cells making up the batteries it will immediately open all relays and signal a fault to the vehicle controller, which will alert the driver. The 12V system has a small lead-acid battery for back-up in the case of an emergency, allowing the vehicle controller to alert the driver of the error. This battery also allows the headlight and taillights to operate for a period of time.

Most of the electrical components are located in the front storage rack of the ATV as shown in Figure 4.12. The components not located in the front rack are the main relay and fuse which are shown in Figure 4.13. The complete electrical system located in storage rack can be quickly disconnected and the entire rack can be removed to allow for easier access to the batteries. Table 4.1 is a listing by letter of the components located in Figure 4.12 and Figure 4.13.

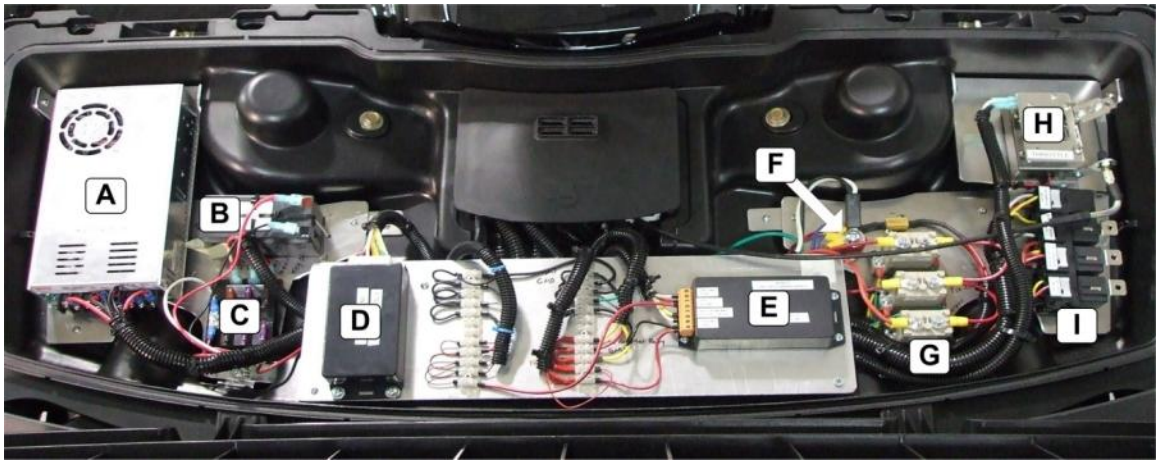

Figure 4.12 - Electrical components in the front rack of the ATV

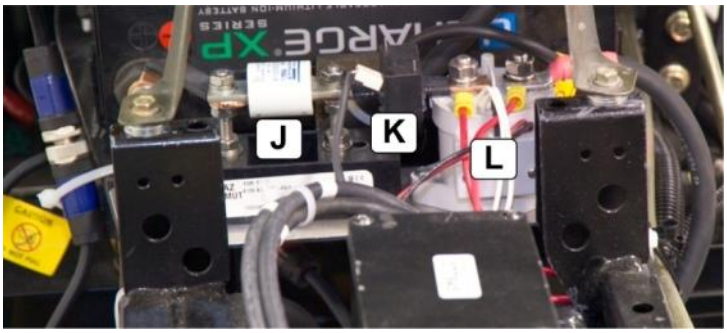

Figure 4.13 - 96V fuse and relay

Table 4.1 - Electrical component description

Component Letter	Description
A	96V to 12V isolated dc/dc converter
B	12V back-up lead acid battery
C	12V system fuses
D	12V to 5V logic interface unit
E	Fuel gauge interface unit
F	96V isolated ground
G	96V relays: pre-charge, charger and auxiliary
H	Throttle potentiometer
I	12V auxiliary relays
J	300A semiconductor fuse
K	DC bus hall effect current sensor
L	96V main relay

The 96V main relay (C3) is an EV200 from Tyco and is capable of continuously carrying a current of 500A and is able to interrupt a current of 2000A. Ideally the control system will keep the current through the relay below its rated values. However, it may be called upon to open while under rated motor current or approximately 150A on the dc-bus. In the case of a short circuit in the cabling, or a short on a leg of the VSC, the fast acting 300A semiconductor fuse will open to protect the batteries from catastrophic failure.

4.5 Vehicle Controller

The vehicle controller shown in Figure 4.14 is a 16-bit digital signal controller (DSC) manufactured by Microchip. The DSC is a combination of a fixed point DSP and a micro-controller. The DSC contains the required peripheral for motor control such as a pulse width modulation (PWM) generator, an analog to digital converter (ADC) and various communication options of which RS-232 is used. The PWM peripheral includes programmable dead-time insertion to prevent both the upper and lower switches in a leg from turning on at the same time. The ADC peripheral is enabled to simultaneously sample the phase currents at the centre of the PWM period, eliminating time delays in the measurement of the different phase currents.

The programming and development environment for the DSC is MPLAB, provided by the manufacturer. The main program flow is coded in C. The integration of fixed-point DSP functionality allows for efficient calculation of math operations, although this functionality required programming in assembly. The main program flow is coded in C with math functions coded in assembly.

No efficient math libraries exist for the DSP and consequently, custom math functions were coded in assembly for the application. The custom library includes functions for calculating the phase and magnitude of two-orthogonal vectors, a park-transform and a custom proportional and integral (PI) control block. The phase of the vectors is calculated using a self normalizing arc-tan from [25]. The magnitude of the vectors is calculated using a third-order curve fitting algorithm. The PI control block is written using a standard approach to a digital PI from [26].

Figure 4.14 - Vehicle controller

4.6 Additional Systems

The ATV contains additional systems to increase the overall energy efficiency and to allow the function of the ATV to bear a resemblance to the conventional ATV. One such system is an analog fuel gauge interface circuit. Rather than add a secondary display to give the driver feedback on the current state of charge of the batteries, a fuel gauge interface circuit, shown in Figure 4.15, is used. The circuit interfaces the 0 to 5V state-of-charge level from the battery management to the resistance based fuel gauge already located on the speedometer hub through an inverting op-amp circuit.

Figure 4.15 - Fuel gauge interface circuit

To increase the overall efficiency of the ATV the 50W brake and taillights were replaced with equivalent brightness 1W LEDs. The 50W headlights were also changed to 1W bright white LEDs that are available as aftermarket on-road vehicle fog lamps. A reflector designed for the LEDs would have to be installed, replacing the existing reflector, in order to increase the illumination depth provided by the LEDs and to compare closer to the original headlights. By changing the five lights on the ATV from halogen to LEDs, the power consumption was reduced from 250W to 5W. This small savings of electrical energy could amount to an extra kilometre or two in drive time over the charge of the battery.

A side profile of the completed ATV is shown in Figure 4.16, without looking very closely at the completed ATV one would not know that is was an electric version of the popular gasoline powered Polaris Sportsman ATV. The front of the ATV is shown in Figure 4.17 in which the bluish glow of the LED headlights is visible. The red glow of

LED brake lights is also visible in Figure 4.18, also notice the motor drive enclosure and its heat sink under the back rack.

Figure 4.16 - The side profile of electric ATV prototype

Figure 4.17 - The front of the electric ATV prototype

Figure 4.18 - The back of the electric ATV prototype

5 MODEL VALIDATION

5.1 Overview of Laboratory Tests

In order to confirm the correct operation of the digital signal controller implemented control system and to confirm the simulation results from PSCAD a test bench as shown in Figure 5.1 is used. The prototype ATV is lifted from the ground using four jack-stands to allow both axles to spin freely. To simulate a load on the ATV the brake is applied. The more the brake is applied, the greater the simulated load on the vehicle. This testing procedure is used primarily due to the limited portability of the lab equipment used for recording the waveforms. The testing method reduces the amount of uncontrolled variables such as wind effect, road grade load and rolling resistance of the terrain types.

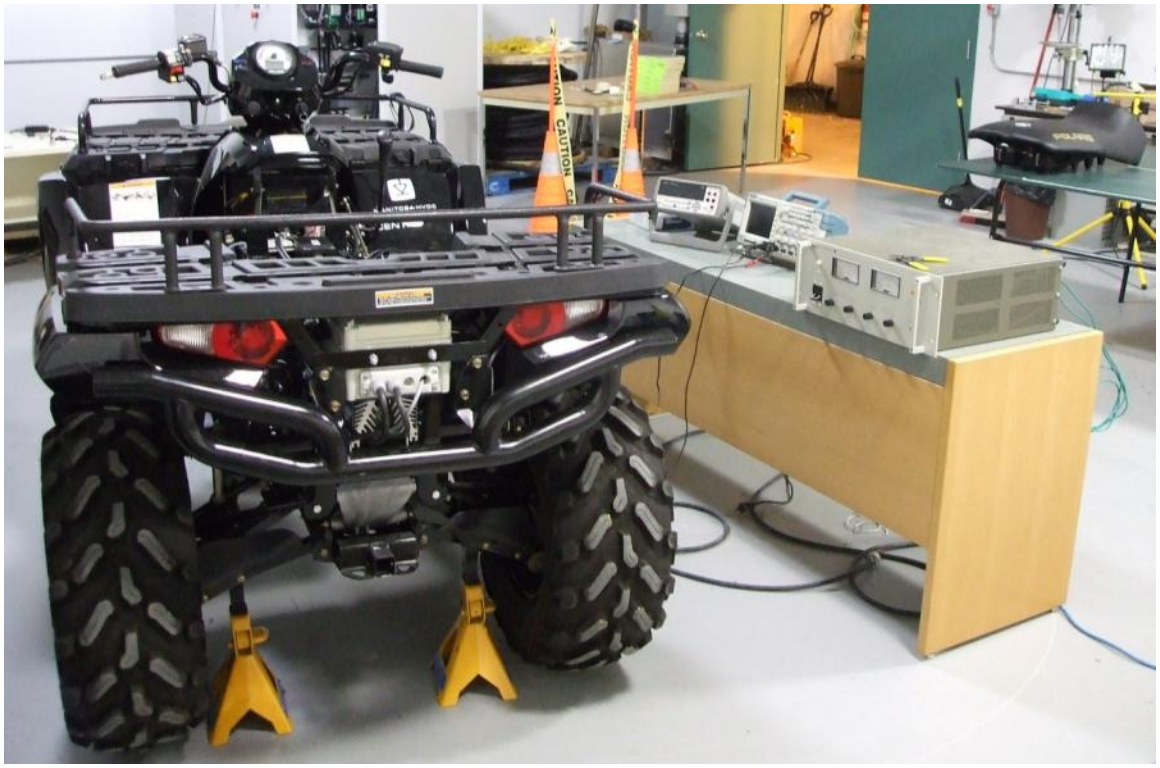

Figure 5.1 - ATV jack-stand test bench setup

The PSCAD simulation case is modified to allow for direct comparisons to the lab test setup. The vehicle will not be moving through the air therefore, the coefficient of aerodynamic drag is set to zero. As there will be no rolling resistance due to the tire to ground interacting, the rolling resistance coefficient is reduced to equal the mechanical losses of the overall system obtained during the testing. Two tests are performed with each testing being performed at multiple operating points. These tests are vehicle speed tests and varying brake load tests.

5.2 Vehicle Speed Tests

The vehicle speed tests are performed at increments of 5km/hr starting at 5km/hr and ending at 45 km/hr. These tests help to confirm the response of the control system at

different operating points. The resulting currents should be sinusoidal and the values should match closely the predicted values from simulation. Figure 5.2 shows the trend of current versus speed for both the PSCAD simulation case and the measured prototype current, a single test at each speed was recorded. At lower speeds the values are essentially identical, as the speed is increases above 25 km/hr the prototype consistently draws higher values of current. This can be partially explained by the wheel spinning in the air. The PSCAD load model only accounts for a linear increase in the rolling resistance with speed, where as the effects of the tires spinning in the air increases the overall loading on the prototype. The higher load currents at higher speeds are a result of this increased loading.

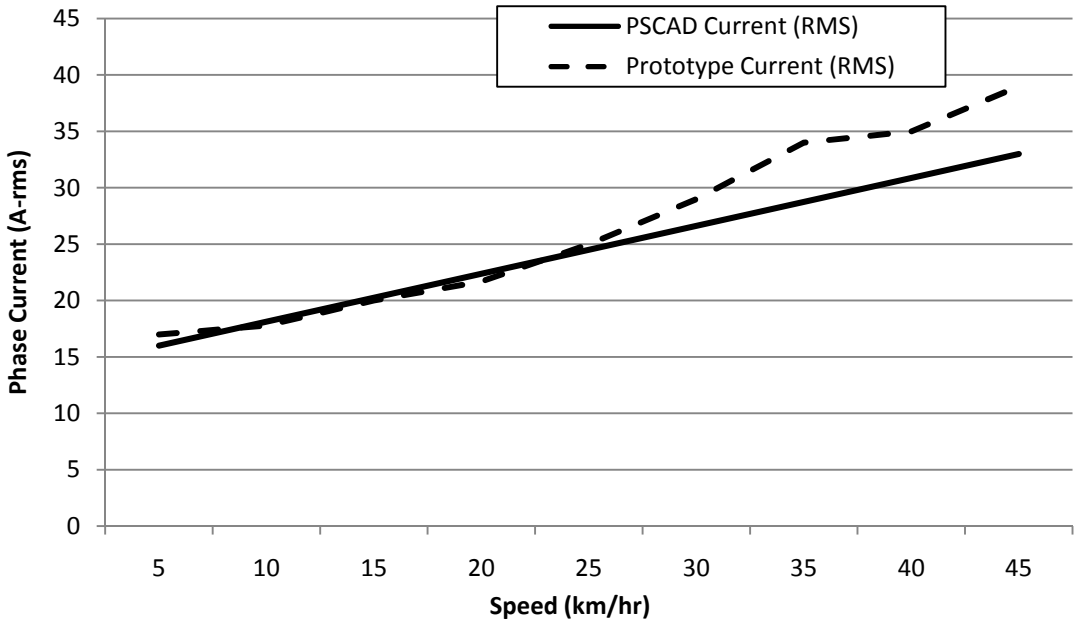

Figure 5.2 - Trend speed versus motor current (RMS)

Figure 5.3 and Figure 5.4 show the results of speed tests at both 10 km/hr and 45km/hr respectively. The increases in the electrical frequencies are as expected from the simulation case. At higher speeds the effects of the mechanical system start to have effects on the response of the motor. To achieve the sharp angle and large amount of suspension travel, the mechanical universal joints have added play. This looseness of the joints can be heard when running the tests as a low banging resulting in a transient change in the overall loading. This change in load is more evident at higher speeds as can be observed by the changes in the load current in Figure 5.4. The first cycle's peak is lower than the second cycle's peak. These effects are also visible in the next set of tests.

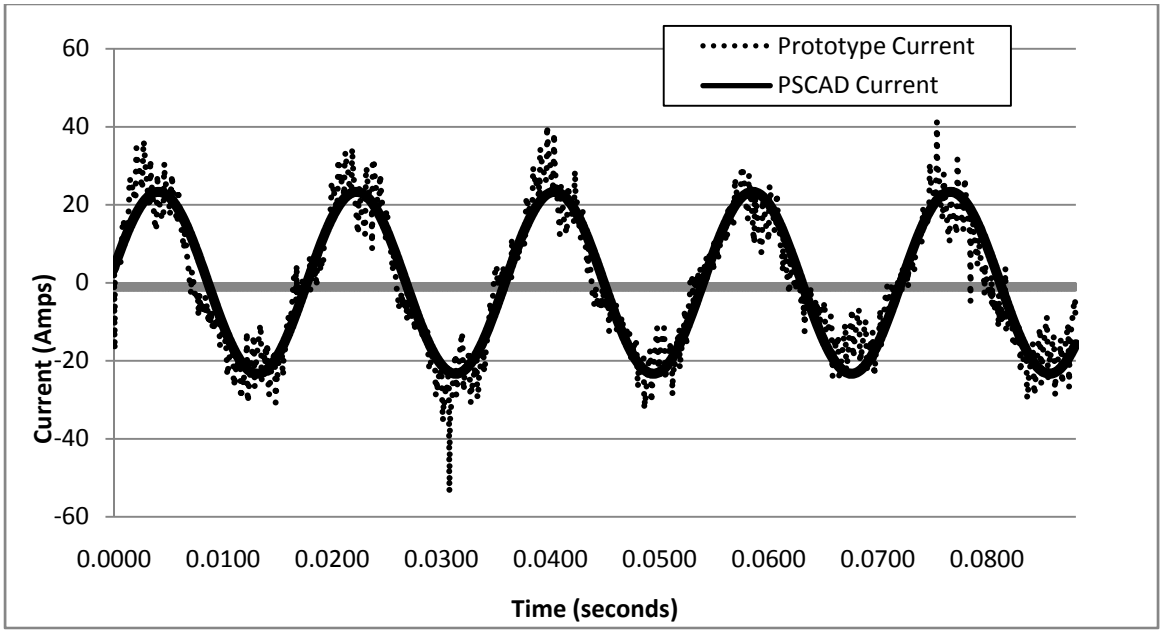

Figure 5.3 - Speed test for 10km/hr

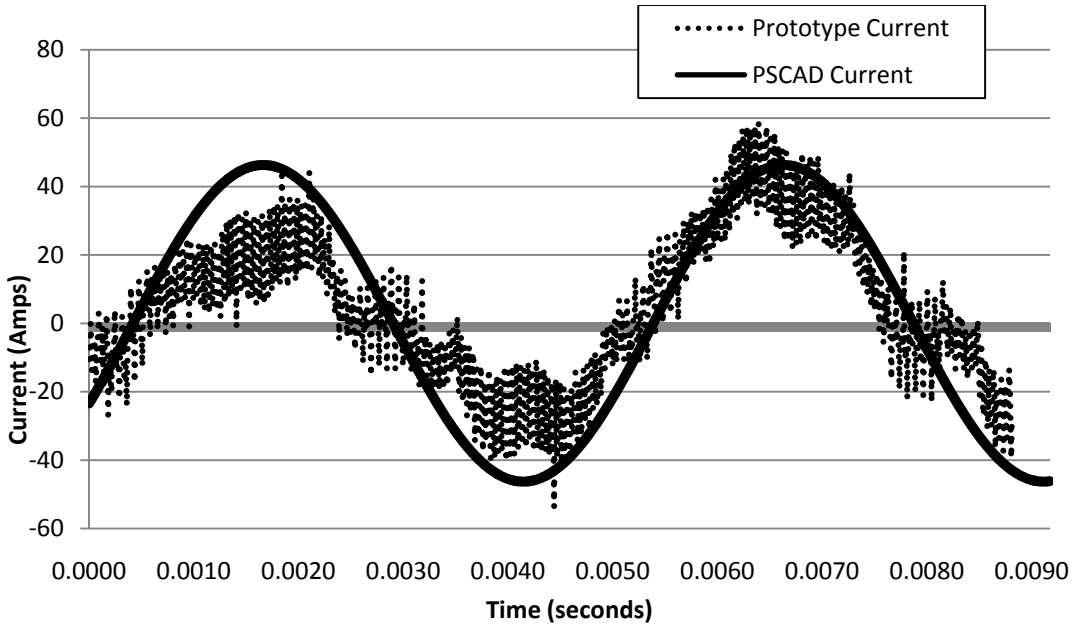

Figure 5.4 - Speed test for 45 km/hr

5.3 Varying Brake Load Tests

To determine the control system's ability to adapt to varying load conditions the brake is used to vary the load on the vehicle. As the operating point of the control system is set by the amount the throttle is depressed. Two-actions are undertaken to perform this test. The vehicle is smoothly accelerated until a speed of 25km/hr is achieved. At this point the brake is applied gradually while the throttle is further depressed to maintain vehicle speed of 25km/hr. Three different loading points are performed, one each at 50A, 70A and 78A of RMS line current. The results of these tests are shown in Figure 5.5, Figure 5.6 and Figure 5.7 respectively. The perturbations in the current waveforms, including phase shifts, are primarily a result of the transiently changing mechanical load as described in the previous section.

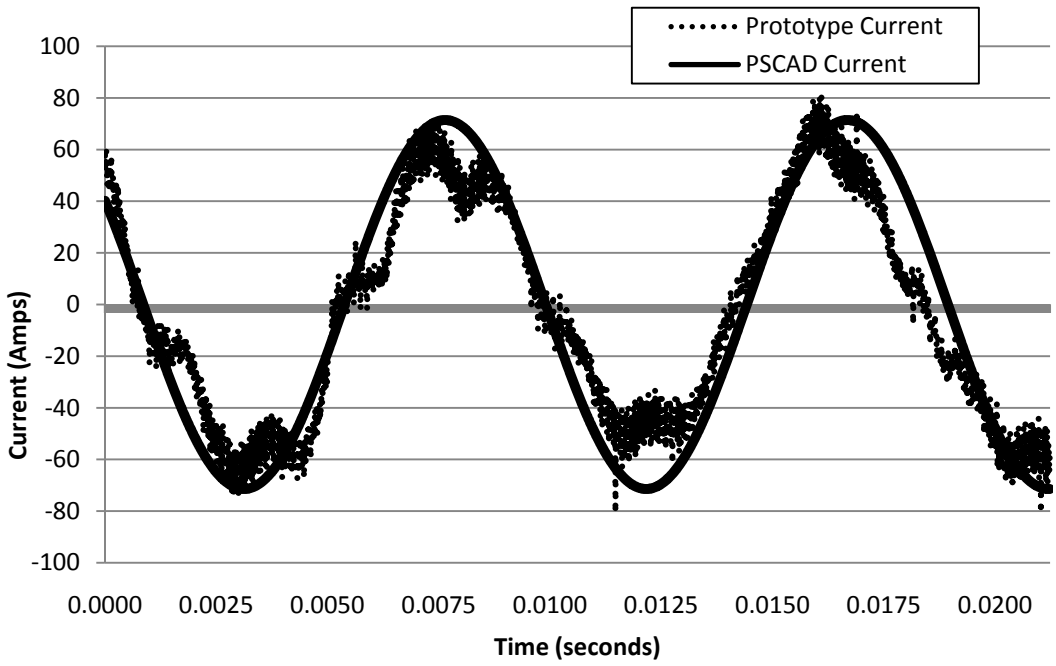

Figure 5.5 - Current waveforms for load current of 50A at 25km/hr

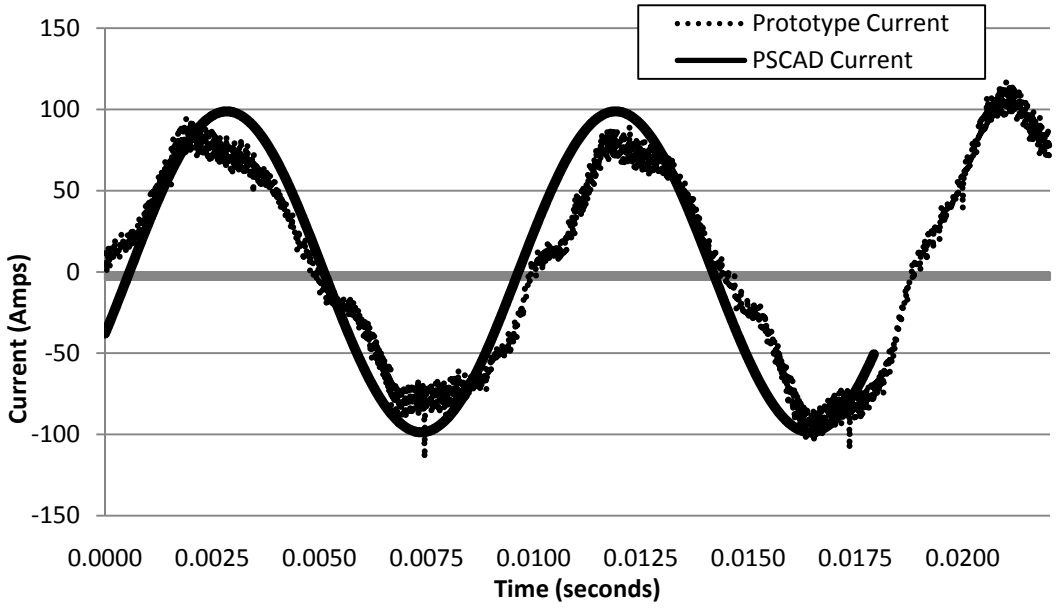

Figure 5.6 - Current waveform for load current of 70A at 25km/hr

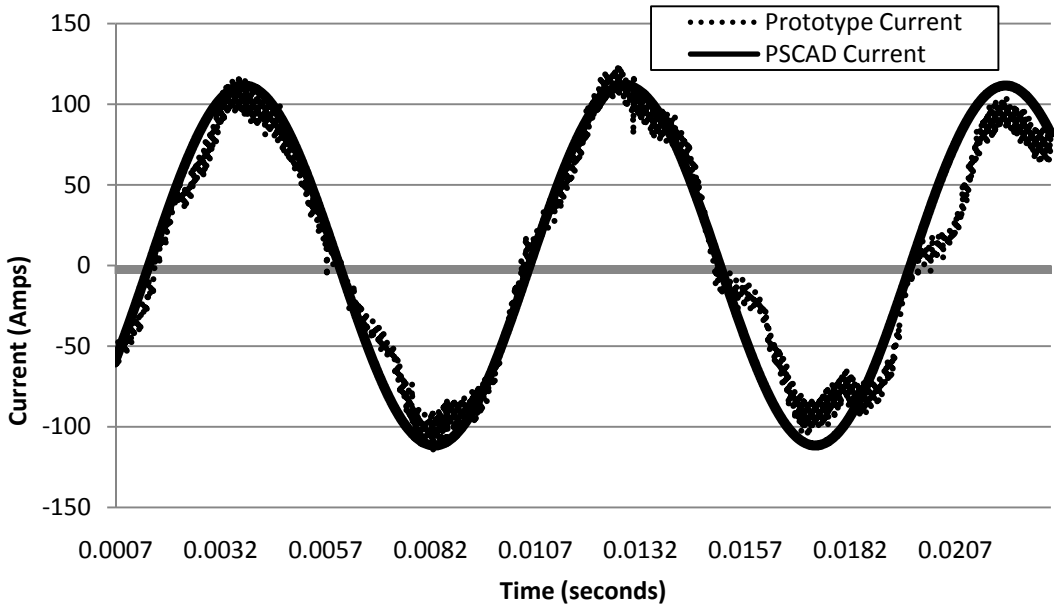

Figure 5.7 - Current waveform for load current of 78A at 25 km/hr

5.4 Road Test

Final acceleration tests were performed on asphalt due to the limited accessibility of different testing environments. To reduce the risk of destroying the power electronics during testing the current through the power electronic switches was limited to 100 A_{rms}. Acceleration tests were performed multiple times in both high and low gears. One of the low gear acceleration tests is shown in Figure 5.8 and one of the high gear acceleration tests is shown in Figure 5.9, each being compared to a PSCAD simulation under similar conditions.

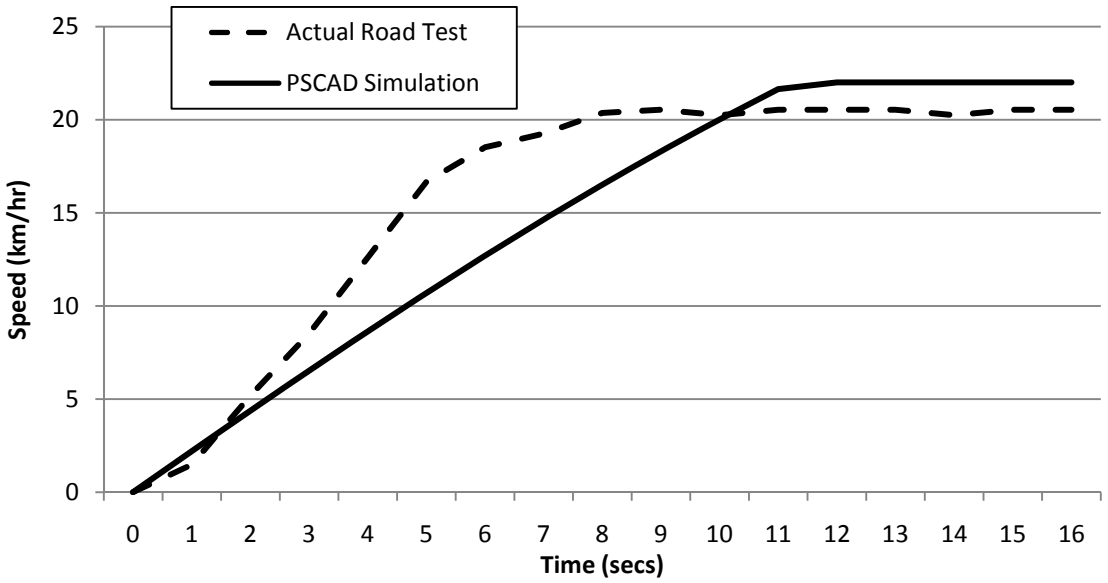

Figure 5.8- Comparison of real and simulated acceleration test on asphalt in low gear

The speed data from these tests was recorded using a GPS data-logger capable of logging the data at 1 second intervals. Both of the acceleration curves compare well to the PSCAD simulation case. The actual top speed achieved in the low gear test is slightly lower than that of the PSCAD simulation case. This steady state difference is primarily due to the battery model used in PSCAD. The model does not take into consideration the voltage depression at the terminal of the batteries when a large current is extracted from them. The difference in the top speed achieved during the acceleration test in high gear can be attributed to a slight elevation in the grade during the tests.

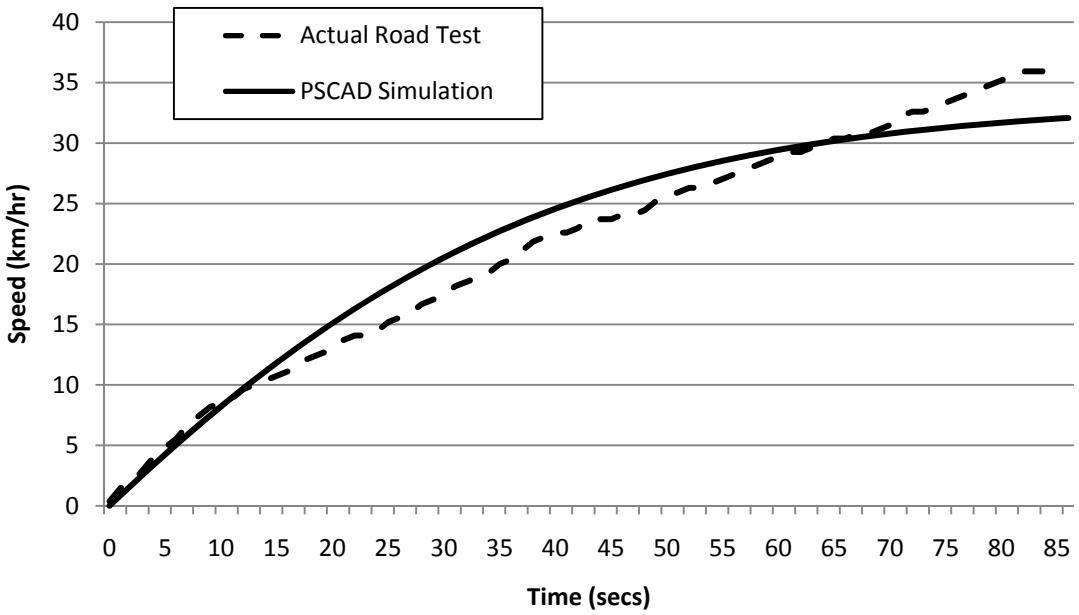

Figure 5.9 - Comparison of real and simulated acceleration test on asphalt in high gear

5.5 Testing Summary

Throughout all the tests the control system maintains its ability to both sustain and limit the current to the requested value. If the load on the vehicle is increased the vehicle begins to lose speed, unless the current request is increased by depressing the throttle further. If the load on the vehicle is reduced, the vehicle begins to accelerate unless the throttle is reduced. The tests demonstrate that the developed torque control system responds similarly to a conventional gasoline powered ATVs satisfying the requirement set out in Chapter 3.

6 CONCLUSIONS AND RECOMMENDATIONS

6.1 Contributions

The thesis has discussed the development of an electric ATV. The initial design was undertaken in a transient simulation program (PSCAD) which allowed for a complete software model of both the mechanical and electrical systems. This simulation allowed for the optimization of the control system parameters. Using results from the simulation, a prototype was then constructed to compare and evaluate the results. The following points are further details of the contributions of this work.

1. An electromagnetic transient simulation was undertaken using PSCAD. Standard library components combined with a detailed custom written vehicular load model were used for the initial component selection.
2. Optimization of the control parameters was obtained using the simulation model and a non-linear simplex optimization routine.
3. A prototype vehicle was constructed using components, such as an electrical traction motor and batteries that were selected from the simulation results. The prototype vehicle includes a customized motor drive whose ratings and control parameters were selected with the aid of the simulation studies.
4. Custom control blocks were also implemented within PSCAD to emulate the limited mathematical capabilities of a digital signal controller. These blocks in turn aided in the programming and further tuning of the controller.

5. Limited testing of the vehicle was performed to compare the results of the PSCAD simulation case to the prototype vehicle with reasonable control system results obtained.

6.2 Future Work

To increase the performance of the vehicle and to aid in future vehicle and motor control projects the following items are recommended as future work:

1. Integrating the ability to directly program micro-controllers and DSP from a completed PSCAD simulation case. This would reduce the time requirements and simplify the development of motor drives and their controllers. This would also allow for more efficient tuning of the controllers.
2. The implementation of a detailed battery model. This would allow for a more comprehensive control system to be built that would include better abilities to function through the voltage depressions and oscillations that occur with high current draws. Having the ability to model aging effects and state-of-charge effects would allow for comparison of battery technologies.
3. The inclusion of regenerative braking on the ATV would allow for the study of the increase in energy efficiency that can be obtained using this feature.

In summary the conversion of a conventional gasoline ATV to an electric ATV was completed. The component ratings and selection was accomplished by using the results of a detailed electromagnetic transient simulation program, PSCAD. The prototype design offers the same control as a conventional ATV. The results of the simulation correlate well with the measured results of the prototype control system. Finally,

simulation using PSCAD has been an effective tool in the design stage of an electric vehicle.

7 REFERENCES

[1] Natural Resources Canada. *Canadian Vehicle Survey*. Energy Publications – Office of Energy Efficiency, 2007.

[2] J. Laeminie and J. Lowry, *Electric Vehicle Technology Explained,* UK: John Wiley & Sons, 2003.

[3] A. F. burke, "Batteries and ultracapacitors for electric, hybrid and fuel cell vehicles." *Proceedings of the IEEE,* vol. 95, pp806-820, April 2007.

[4] C. C. Chan, Y. S. Wong, "Electric vehicles charge forward," *IEEE Power and Energy Magazine*, vol. 2, iss. 6, pp. 24-33, Nov-Dec. 2004.

[5] "Honda ATV History – The 1960s: Prototyping the ATC." Internet: www.hondanews.com/categories/512/releases/2380, Nov. 22, 2004 [July 17,2008].

[6] C. C. Chan, "The state of the art of electric vehicles technology," *Proceedings of the IEEE,* vol. 90, pp247-275, Feb 2002.

[7] J. M. Miller, *Propulsion Systems for Hybrid Vehicles,* UK: IEE, 2004.

[8] P. C. Sen, *Principles of Electric Machines and Power Electronics*, *2nd Edition*, Toronto: John Wiley & Sons, 1996.

[9] B. K. Bose, *Modern Power Electronics and AC Drives*, Upper Saddle River, NJ: Prentice Hall, 2002.

[10] M. Ehsani, Y. Gao, S. E. Gay and A. Emadi, *Modern Electric, Hybrid Electric, and Fuel Cell Vehicles, Fundamentals, Theory and Design.* New York: CRC Press, 2005.

[11] J. M. Miller, "Hybrid electric vehicle propulsion system architectures of the e-CVT type," *IEEE Trans. On Power Electronics,* vol 21, pp 756-767, May 2006.

[12] A. Stone, "How to Build a Quick-Charging Electric Battery." Internet: http://www.forbes.com/technology/2008/01/12/electric-cars-nanotech-tech-sciences-cz_as_0112nano.html, Jan. 18, 2008 [June 12, 2008].

[13] M. Ceraolo, G. Pede, "Techniques for estimating the residual range of an electric vehicle," *IEEE trans. On Vehicular Technology,* vol. 50, pp. 109-115. Jan 2001.

[14] C. Rosenkrans, "Deep cycle batteries for plug-in hybrid application," EPRI hybrid electric vehicle working group, Nov. 15, 2003.

[15] J. Y. Wong, *Theory of Ground Vehicles*. Toronto: John Wiley & Sons, 2001.

[16] M. Ehsani, Y. Gao, S. E. Gay, A. Emadi, *Modern Electric, Hybrid Electric and Fuel Cell Vehicles, Fundamentals, Theory and Design.* New York: CRC Press, 2005

[17] T. J. Akai, *Applied Numerical Methods for Engineer,* Toronto: John Wiley & Sons, 1994.

[18] P. C. Krause, O. Wasynczuk, S. D. Sudhoff, *Analysis of Electric Machinery and Drive Systems*, New York: John Wiley and Sons, 2002.

[19] G. Gallegos-Lopez, F. S. Gunawan, J. E. Walters, "Optimum Torque Control of Permanent-Magnet ac Machines in the Field-Weakened Region." *IEEE trans. on industry applications*, vol 41, pp1020-1028, July/August 2005.

[20] J. F. Giera, R. Wang, M. J. Kamper, *Axial Flux Permanent Magnet Brushless Machines,* Boston: Kluwer Academic, 2004.

[21] J. Sun, H. Grotstollen, "Optimized Space Vector Modulation and Regular-Sampled PWM: A Reexamination," in *Thirty-First Industrial Applications Conference and Annual Meeting, 1996, pp 956-963.*

[22] *EMTDC Manual*, Manitoba HVDC Research Centre, April 2004.

[23] L. Gao, S. Liu, R. A. Dougal, "Dynamic Lithium-Ion Battery Model for System Simulation." *IEEE trans. on componenets and packaging technologies,* vol. 25, pp 495-505, September 2002.

[24] A. M. Gole, S. Filizadeh, R. W. Menzies, P. L. Wilson, "Optimization-enabled electromagnetic transient simulation," *IEEE trans. power delivery,* vol. 20, pp 512-518, Jan. 2005

[25] "Fixed-Point Atan2 with Self Normalization" Internet: www.dspguru.com/comp.dsp/tricks/alg/fxdatan2.htm, April. 4, 1999 [March 20, 2008].

[26] G. F. Franklin, J. D. Powell, M. Workman, *Digital Control of Dynamic System,* California: Addison Wesley Longman Inc, 1998.